

Nuclear shadowing in deep inelastic scattering on nuclei: leading twist versus eikonal approaches

L. Frankfurt

*Nuclear Physics Dept., School of Physics and Astronomy,
Tel Aviv University, 69978 Tel Aviv, Israel
E-mail: frankfur@lev.tau.ac.il*

V. Guzey

*Special Research Centre for the Subatomic Structure of Matter (CSSM),
Adelaide University, 5005, Australia,
vguzey@physics.adelaide.edu.au*

M. McDermott

*Division of Theoretical Physics,
Dept. Mathematical Sciences, Liverpool University
Liverpool L69 3BX, England
E-mail: martinmc@amtp.liv.ac.uk*

M. Strikman

*Department of Physics, Penn State University,
University Park, PA, 16802-6300, USA.
E-mail: strikman@phys.psu.edu*

ABSTRACT: We use several diverse parameterizations of diffractive parton distributions, extracted in leading twist QCD analyses of the HERA diffractive deep inelastic scattering (DIS) data, to make predictions for leading twist nuclear shadowing of nuclear quark and gluon distributions in DIS on nuclei. We find that the HERA diffractive data are sufficiently precise to allow us to predict large nuclear shadowing for gluons and quarks, unambiguously. We performed detailed studies of nuclear shadowing for up and charm sea quarks and gluons within several scenarios of shadowing and diffractive slopes, as well as at central impact parameters. We compare these leading twist results with those obtained from the eikonal approach to nuclear shadowing (which is based on a very different space-time picture) and observe sharply contrasting predictions for the size and Q^2 -dependence of nuclear shadowing. The most striking differences arise for the interaction of small dipoles with nuclei, in particular for the longitudinal structure function F_L^A .

KEYWORDS: Deep Inelastic Scattering, QCD, Hadronic Colliders, Phenomenological Models.

Contents

| | |
|---|-----------|
| 1. Introduction | 1 |
| 2. The leading twist and eikonal approaches to nuclear shadowing | 4 |
| 2.1 The leading twist approach | 4 |
| 2.1.1 The master formulae for leading twist nuclear shadowing | 4 |
| 2.1.2 The transition between shadowing and antishadowing: setting $x_{\mathcal{P},0}$. | 10 |
| 2.1.3 Numerical predictions for nuclear PDFs and F_2^A | 11 |
| 2.1.4 Predictions for central collisions | 21 |
| 2.2 The eikonal approximation approach | 22 |
| 2.3 Differences between the leading twist and eikonal approaches | 27 |
| 3. Nuclear shadowing of the longitudinal structure function F_L^A | 29 |
| 4. Conclusions and discussion | 32 |
| A. Parameterizations of diffractive parton distributions and σ_{eff} | 34 |
| B. Parameterization of the nuclear one-body density | 40 |

1. Introduction

The high-energy scattering of leptons and hadrons from nuclear targets offers a unique possibility to study the distribution of quarks and gluons in nuclei, i.e., large parton densities in a large volume. It is now firmly established by several experiments (EMC and NMC at CERN, a number of experiments at SLAC, E665 at Fermilab) that at small values of Bjorken x , $5 \times 10^{-3} \leq x \leq 0.03 - 0.07$ (for $Q^2 \geq 1 \text{ GeV}^2$), the inclusive nuclear structure function, F_2^A , for DIS on a nucleus with A nucleons, is smaller than the incoherent sum of the nucleon structure functions, AF_2^N . This phenomenon is called nuclear shadowing (for recent reviews see [1]). It is important to emphasize that the available data, which admittedly has a rather limited kinematic range, $Q^2 \lesssim 4 \text{ GeV}^2$, demonstrate no significant Q^2 -dependence of nuclear shadowing. In addition, nuclear shadowing of the antiquark distributions has been observed in the Drell-Yan process [2], in the range $0.02 \lesssim x \lesssim 0.05$ and $16 \lesssim Q^2 \lesssim 35 \text{ GeV}^2$. In other words, the data are consistent with the dominance of leading twist shadowing.

Why is it still interesting to work on the subject of nuclear shadowing in DIS on nuclei after the topic has been investigated so thoroughly? There are several reasons.

Firstly, an accurate evaluation of nuclear shadowing is vitally important for both light and heavy nuclei to pin down the nuclear parton distributions. These form the boundary

conditions for hard processes in electron-nucleus DIS experiments proposed in the USA (the electron-ion collider (EIC)) [3] and at DESY [4], in nucleus-nucleus and nucleon-nucleus collisions presently under way at BNL, and in proton-nucleus and nucleus-nucleus collisions planned for the LHC at CERN.

Secondly, it is important to understand the intricate interplay of perturbative and non-perturbative effects in nuclear shadowing and its role in the parton distributions of nuclei at small x . Understanding this interplay is a key element in determining when the leading twist approximation (implicit in the DGLAP evolution equations) breaks down for sufficiently small x .

Thirdly, because of the deep connection between nuclear shadowing and diffraction in DIS on a nucleon established by V. Gribov [5], accurate measurements of nuclear shadowing should help to discriminate between competing models of diffraction.

The dynamics of nuclear shadowing in DIS at high energies is most transparent in the target rest frame where the virtual photon-nucleus (nucleon) scattering, $\gamma^*(q) + A(P_A) \rightarrow X$, is a time-ordered three-stage process.

Firstly, the photon may be considered to fluctuate into a linear superposition of hadronic components labelled by the basis set $|h_k\rangle$. The components consist of quarks, antiquarks and gluons at small relative transverse distances (and their associated color fields) and of hadronic bound states at large transverse distances. For large center-of-mass energy, W ($W^2 = (q + P_A)^2$), i.e., small Bjorken $x \approx A Q^2/W^2$, the fluctuation occurs a long distance upstream of the nuclear target. The incoming virtual photon (more precisely, the hadronic part of the virtual photon) state $|\gamma^*\rangle$ may be expressed generically as follows

$$|\gamma^*\rangle = \sum_k c_k |h_k\rangle, \quad (1.1)$$

in which the index “ k ” should be understood to be a label which fully specifies the hadronic state (i.e., it includes information about momentum fractions and transverse momentum of the constituent partons, their helicities, etc.) and $c_k = \langle h_k | \gamma^* \rangle$.

Secondly, the hadronic configurations $|h_k\rangle$ interact strongly with the nucleus

$$\sigma_{\gamma^* A} = \sum_{k,k'} \hat{c}_{k'}^* \hat{\sigma}_{k,k'}^A c_k, \quad (1.2)$$

where the subprocess cross section, $\hat{\sigma}_{k,k'}^A$, is related via the optical theorem to the imaginary part of the forward scattering amplitude for the process $h_k + A \rightarrow h_{k'} + A$ normalized such that $\hat{\sigma}_{k,k}^A = \sigma_{h_k A}$, the total h_k -nucleus cross section.

Finally, the hadronic final state X is formed.

In general, each state h_k suffers attenuation: at sufficiently high energies the states $|h_k\rangle$ interact coherently with several nucleons of the target. These multiple interactions decrease $\hat{\sigma}_{k,k'}^A$ relative to the sum of $\hat{\sigma}_{k,k'}^N$ of the individual nucleons, which can be translated to the corresponding inclusive structure functions as $F_2^A/(A F_2^N) < 1$. Thus, the coherent interaction of the photon with several nucleons of the target nucleus invariably results in nuclear shadowing.

Equations (1.1,1.2) are very general. Any particular realization requires some modelling of the hadronic content of the (virtual) photon and of the interaction with the target. There are several models in the literature including Generalized Vector Meson Dominance (GVMD) models [6], two-phase models including vector mesons and the Pomeron [7] or other scaling contributions [8], and the QCD-improved aligned jet model [9]. In this paper, we review and compare the two most recent approaches to nuclear shadowing: the leading twist and eikonal approaches.

The leading twist approach was developed in a recent work by Frankfurt and Strikman [10], who attempted to place the treatment of nuclear shadowing on firmer ground. The authors generalized the Gribov theory of nuclear shadowing in hadron-nucleus scattering [5] to individual quark and gluon nuclear parton densities in light nuclei, probed in DIS on nuclei. As in the Glauber model, nuclei were treated as a dilute nucleon gas. The connection between nuclear shadowing in inclusive DIS on the nucleus and diffraction in DIS on the proton, the factorization theorem for hard diffraction [11] and high accuracy DIS diffractive data allowed the leading twist (LT) component of the nuclear shadowing correction to nuclear parton distributions to be evaluated reasonably well. One immediate and very distinct consequence of the theory is that, at some initial scale Q_0 ($Q_0 = 2$ GeV in [10]), nuclear shadowing for gluons is much larger than that for quarks (by a factor of about two or three for the lightest nuclei) because the diffractive structure functions are dominated by gluons.

Another popular approach to nuclear shadowing is the eikonal approximation. This method is based on the assumption that the interaction between the fluctuation $|h_k\rangle$ and nucleons of the target leaves the fluctuation unchanged (i.e., the interaction is diagonal in the appropriate variables). This allows the subprocess to be iterated and summed so that the $|h_k\rangle$ -nucleus total cross sections, $\sigma_{h_k A}$, entering Eq. (1.2) via $\hat{\sigma}_{k,k'}^A$, can be expressed in an exponential form via the *total* $\sigma_{h_k N}$ cross sections. This procedure is termed eikonalization, hence the name of the approximation.

The profound conceptual difference between the leading twist and eikonal approaches is readily revealed by including QCD evolution. Indeed, in QCD quark-antiquark pairs and gluons are radiated by the partons constituting the fluctuations $|h_k\rangle$ before and during the interaction with the target, so that the fluctuations $|h_k\rangle$ necessarily mix. This is included in the leading twist approach and ignored in the eikonal approximation. As a result, the two considered approximations predict a different size and Q^2 -dependence of the shadowing correction. For example, the longitudinal structure function F_L^A is very sensitive to the mixing of the $q\bar{q}$ and $q\bar{q}g$ fluctuations of the incoming photon and thus can serve as a sensitive observable to distinguish between the leading twist and eikonal approximation predictions.

At the outset, it may be useful to clarify the relation of this work to a number of works on the small- x scattering off nuclei (for nice pedagogical reviews and references to original papers, see e.g., [12]). We are working in a kinematic region in which the leading twist contribution dominates diffraction and one has to take into account logs of Q^2 and one or two logs of x_0/x in the evolution of the parton distributions. This can be accounted for by the NLO DGLAP evolution equations. The approaches of [12] focus on a resummation of

the logs of x_0/x (cf. the BFKL approximation) which is not necessary for this kinematic region and neglect certain logs of Q^2 .

This paper is organised as follows. In section 2 we review the leading twist approximation for nuclear shadowing and give predictions for the quark and gluon nuclear densities and for the nuclear structure functions F_2^A , using as input a broad range of leading twist diffractive parton distribution functions (DPDFs), which successfully describe the HERA hard diffraction data. We also review the eikonal approximation approach to nuclear shadowing and discuss various serious problems associated with it. We dedicate section 3 to the longitudinal nuclear structure function, F_L^A , which is predicted to be very different within the two approaches, and indicates general qualitative patterns of contrasting behaviour for hard processes. Discussions and conclusions are presented in section 4. In appendix A we specify and compare the different parameterizations of the DPDFs and observe that, in spite of significant differences in the details of these, they all lead to fairly similar probabilities for quark-induced and gluon-induced diffraction and nuclear shadowing at small x . We also observe that all of these parameterizations lead to a very large probability of leading twist diffraction in gluon-induced processes, which is comparable to the black-body limit of 50% for $x \leq 10^{-4}$ at $Q^2 \sim 4 \text{ GeV}^2$. Finally, the parameterization of the nuclear one-body density for a range of nuclei considered is given in appendix B.

2. The leading twist and eikonal approaches to nuclear shadowing

In this section we review both the leading twist and eikonal approaches to nuclear shadowing (subsections 2.1 and 2.2). A critical comparison of the approaches is presented in subsection 2.3.

2.1 The leading twist approach

The basis of our present day understanding of nuclear shadowing in high-energy scattering on nuclei was formulated in the seminal work by V. Gribov [5]. The key observation was that, within the approximation that the radius of the strong interactions is much smaller than the average inter-nucleon distances in nuclei, there is a direct relationship between nuclear shadowing in the total hadron-*nucleus* cross section and the cross section for diffractive hadron-*nucleon* scattering. While the original derivation was presented for hadron-deuterium scattering, it can be straightforwardly generalized to lepton-nucleus DIS.

2.1.1 The master formulae for leading twist nuclear shadowing

In this subsection we aim to motivate a master formula which relates nuclear shadowing to diffraction off a single nucleon and includes the scattering off an arbitrary number of nucleons. The main result of the work by Frankfurt and Strikman [10] is the observation that the Gribov theory can be generalized to calculate the leading twist component of nuclear shadowing for each nuclear parton distribution *separately*. We shall review the principal steps of the derivation below. The starting point is the generalization of Gribov's result to DIS of leptons on deuterium. The nuclear shadowing correction to the deuteron

structure function, $\delta F_2^D = F_2^p + F_2^n - F_2^D$, where F_2^D , F_2^p , F_2^n are the deuteron, proton, neutron structure functions, respectively, can be presented in the form

$$\delta F_2^D(x, Q^2) = 2 \frac{1 - \eta^2}{1 + \eta^2} \int dk_t^2 dx_{\mathcal{P}} F_2^{D(4)}(\beta, Q^2, x_{\mathcal{P}}, k_t^2) F_D(4k_t^2 + 4x_{\mathcal{P}}^2 m_N^2). \quad (2.1)$$

Here $F_2^{D(4)}$ is the diffractive structure function of the proton in terms of the usual diffractive variables, $Q^2 = -q^2$, $\beta \equiv -q^2/(2q \cdot k) \equiv Q^2/(Q^2 + M_X^2 - k^2) \approx Q^2/(Q^2 + M_X^2)$ and $x_{\mathcal{P}} \equiv 2q \cdot k/(2q \cdot p) \equiv x/\beta \approx (Q^2 + M_X^2)/(2p \cdot q)$; k_t is the transverse momentum transfer to the nucleon; η is the ratio of the real to imaginary parts of the diffractive scattering amplitudes¹ for the reaction $\gamma^* + N \rightarrow X + N$; F_D is the deuteron electromagnetic form factor².

The relevant Feynman graph for the forward scattering amplitude of the double scattering diagram is shown in Fig. 1, which also serves to define the four-momentum flow. In particular, the momentum transfer to the proton $k = p' - p$ is mostly transverse³, so that $k^2 \approx -k_t^2$. In order to find the shadowing correction to the total virtual photon-deuteron cross section (and hence δF_2^D) one needs to find the imaginary part of the forward amplitude of the diagram in Fig. 1.

We can also obtain Eq. (2.1) in a somewhat different way than in the original Gribov paper by using the Abramovsky-Gribov-Kancheli cutting rules [14]. Instead of considering directly the imaginary part of the total rescattering amplitude, one can first consider the cross section corresponding to the diffractive cut of the amplitude in Fig. 1 (see Fig. 1 of [10]). In this case, the answer is given by the same diffractive cross section that enters lepton-nucleon diffractive scattering, i.e., the diagram is proportional to $|\text{Im}A|^2 + |\text{Re}A|^2$, where A is the amplitude for diffractive lepton-proton scattering. One then compares the expression for the imaginary part of the forward amplitude of the double scattering diagram to that with the diffractive cut. Using the cutting rules, one observes that the former is proportional to $|\text{Im}A|^2 - |\text{Re}A|^2$, while $F_2^{D(4)}$ is proportional to $|\text{Im}A|^2 + |\text{Re}A|^2$. This explains how the answer for δF_2^D can be expressed in terms of the nucleon diffractive structure functions, $F_2^{D(4)}$, as well as the presence of the factor $(1 - \eta^2)/(1 + \eta^2)$ in Eq. (2.1).

The deuteron form factor arises from the non-relativistic calculation of the overlapping integral of deuteron wavefunctions ψ_D . Indeed, when one nucleon with a three-momentum \vec{p} receives a three-momentum $\vec{k} = (\vec{k}_t, k_3 \approx m_N x_{\mathcal{P}})$, the other nucleon with a three-momentum $-\vec{p}$ receives a three-momentum $-\vec{k}$ (see Fig. 1). Hence, the lower (nuclear) part of the diagram in Fig. 1 is proportional to $\int d^3p \psi_D(\vec{p}) \psi(\vec{p} + \vec{k}) = F_D(4k^2)$ because the electromagnetic form factor is defined as $F_D(q^2) \equiv \int d^3p \psi_D(\vec{p}) \psi(\vec{p} + \vec{q}/2)$. When the argument of the form factor is large, i.e., when either $x_{\mathcal{P}} \geq 1/(m_N r_D)$ or $k_t \gg 1/r_D$, the damping of the form factor annihilates δF_2^D (r_D is the average electromagnetic deuteron radius).

¹The factor associated with a non-zero η is absent in the original derivation of [5] since the intercept of the Pomeron trajectory $\alpha_{\mathcal{P}}(0)$ was assumed to be equal to unity, see Eq. (2.3).

²For simplicity we give the expression for the spin-less deuteron. For the spin-one deuteron the relevant form factors were calculated in [13].

³The transverse plane is defined relative to the virtual-photon nucleon center of mass frame. Given that the momentum is mostly transverse, to a very good approximation, we use t and k_t^2 interchangeably.

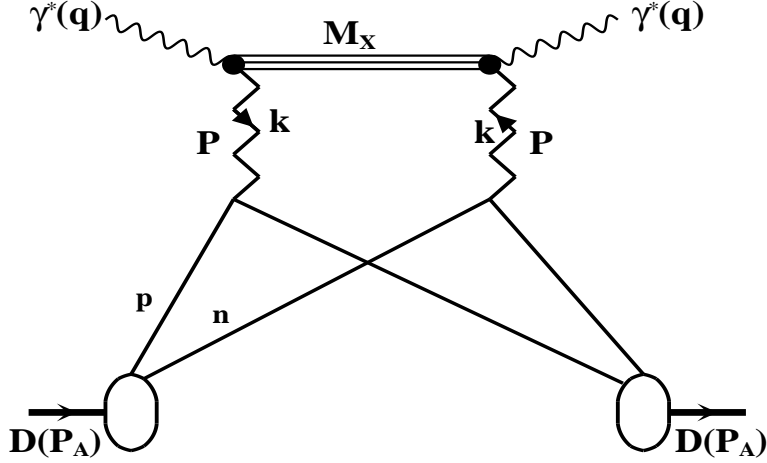


Figure 1: Feynman diagram demonstrating the connection between the nuclear shadowing correction to the deuteron structure function, δF_2^D , and the proton diffractive structure function $F_2^{D(4)}$.

Equation (2.1) can be generalized to DIS on any nucleus. The shadowing correction to the nuclear inclusive structure function, which arises due to scattering on any *pair* of nucleons, $\delta F_2^{A(2)}$, can be written in the form

$$\delta F_2^{A(2)} = \frac{A(A-1)}{2} 16\pi \text{Re} \left[\frac{(1-i\eta)^2}{1+\eta^2} \int d^2b \int_{-\infty}^{\infty} dz_1 \int_{z_1}^{\infty} dz_2 \int_x^{x_{P,0}} dx_P \times \right. \\ \left. F_2^{D(4)}(\beta, Q^2, x_P, k_t^2) \Big|_{k_t^2=0} \rho_A(b, z_1) \rho_A(b, z_2) e^{ix_P m_N (z_1 - z_2)} \right]. \quad (2.2)$$

Here ρ_A is the nuclear one-body density per nucleon normalized such that $\int d^3\vec{r} \rho_A(\vec{r}) = 1$; z_1 and z_2 are the longitudinal coordinates of the two nucleons involved in the scattering; \vec{b} is the impact parameter of the projectile with respect to the center of the nucleus. The upper limit of integration, $x_{P,0}$ will be discussed later in the text. A non-vanishing longitudinal momentum transfer to the target is taken into account by the factor⁴ $\exp(ix_P m_N (z_1 - z_2))$. The implied suppression for large $x_P m_N$ is implicitly included in Eq. (2.1) by the $4x_P^2 m_N^2$ term in the argument of the deuteron form factor.

We determine the ratio of the real to imaginary parts of the diffractive scattering amplitude, η , by assuming a universal exchange and using the analytical properties of the scattering amplitude as a function of energy, as suggested by Gribov and Migdal [16]. Applying the Gribov-Migdal expression to our case, we determine η as a function of the intercept of the Pomeron trajectory, $\alpha_P(0)$,

$$\eta = \frac{\pi}{2} \frac{\partial \ln A}{\partial \ln 1/x} = \frac{\pi}{2} (\alpha_P(0) - 1). \quad (2.3)$$

⁴This factor is analogous to the one which was derived within the vector meson dominance model of photoproduction and electroproduction (for a review see [15]). In the context of DIS it was first introduced in the second reference of [9].

Different values for $\alpha_{\mathcal{P}}(0)$ obtained by various groups correspond to different values for η . In our analysis, we used $\eta = 0.22$ in conjunction with the ACWT parameterization of DPDFs [17] ($\alpha_{\mathcal{P}}(0) = 1.14$) and $\eta = 0.32$ in conjunction with the H1 [18] parameterization ($\alpha_{\mathcal{P}}(0) = 1.20$).

The integration over k_t is absent in Eq. (2.2) since it is assumed that the slope of the elementary diffractive amplitude for the reaction $\gamma^* + N \rightarrow X + N$ is much smaller than the slope of the nuclear electromagnetic form factor⁵. This allows one to replace the diffractive nucleon structure function by its value at $k_t^2 = 0$.

Equations (2.1) and (2.2) include only the spin non-flip part of the diffractive cross section, which is proportional to $F_2^{D(4)}$. Spin-flip effects in diffraction are highly suppressed at small t by the structure of the Pomeron vertex and thus can be safely neglected.

The crucial observation made in [10] was that Eq. (2.2) can be generalized to nuclear parton densities. Indeed, the QCD factorization theorems for inclusive DIS [19] and hard diffraction [11] allow one to express the inclusive and diffractive structure functions, entering the left and right hand sides of Eq. (2.2), respectively, as a convolution of the *same* hard scattering coefficients with the corresponding, i.e., inclusive and diffractive, parton distributions. Equating the terms in front of each hard scattering coefficient, one immediately arrives at the key expression for the shadowing correction to the nuclear parton distributions, $\delta f_{j/A}^{(2)}(x, Q^2)$,

$$\delta f_{j/A}^{(2)}(x, Q^2) = \frac{A(A-1)}{2} 16\pi R e \left[\frac{(1-i\eta)^2}{1+\eta^2} \int d^2b \int_{-\infty}^{\infty} dz_1 \int_{z_1}^{\infty} dz_2 \int_x^{x_{\mathcal{P},0}} dx_{\mathcal{P}} \times \right. \\ \left. f_{j/N}^D(\beta, Q^2, x_{\mathcal{P}}, 0) \rho_A(b, z_1) \rho_A(b, z_2) e^{ix_{\mathcal{P}} m_N (z_1 - z_2)} \right]. \quad (2.4)$$

Here j indicates a generic parton label (i.e., a gluon, or a quark of a particular flavour); $f_{j/N}^D$ is the diffractive parton distribution function (DPDF) of the nucleon⁶, for parton of type j . Equation (2.4) is the main result of [10] and demonstrates the intimate connection between the nuclear shadowing correction to nuclear inclusive parton distribution functions (PDFs) and the DPDFs of the nucleon. Since $f_{j/N}^D$ obeys the leading twist DGLAP evolution equation, the Q^2 -evolution of $\delta f_{j/A}^{(2)}$ is also governed by DGLAP, i.e., it is *by definition* a leading twist contribution. This explains why the approach of [10] can legitimately be called the leading twist approach. However, the validity of Eqs. (2.1,2.2,2.4) does not require the absence of the higher twist effects in diffraction. Hence, as soon as a particular parameterization of the diffractive cross sections fits the data, one can use this parameterization to calculate the shadowing correction to the structure functions, using Eqs. (2.1,2.2,2.4), without addressing the question of decomposition of the diffractive cross section over twists.

⁵This is analogous to the optical model approximation of the Glauber model which is known to work very well for $A \geq 12$.

⁶We do not distinguish between protons and neutrons since we consider small- x scattering in the vacuum channel.

Ignoring for a moment the contribution to nuclear shadowing arising from the interactions with three and more nucleons of the target, the connection of $\delta f_{j/A}^{(2)}$ to nuclear ($f_{j/A}$) and nucleon ($f_{j/N}$) PDFs is given by

$$f_{j/A} = Af_{j/N} - \delta f_{j/A}^{(2)}, \quad (2.5)$$

and is depicted graphically in Figs. 2 and 3 for the up quark and gluon distributions, respectively.

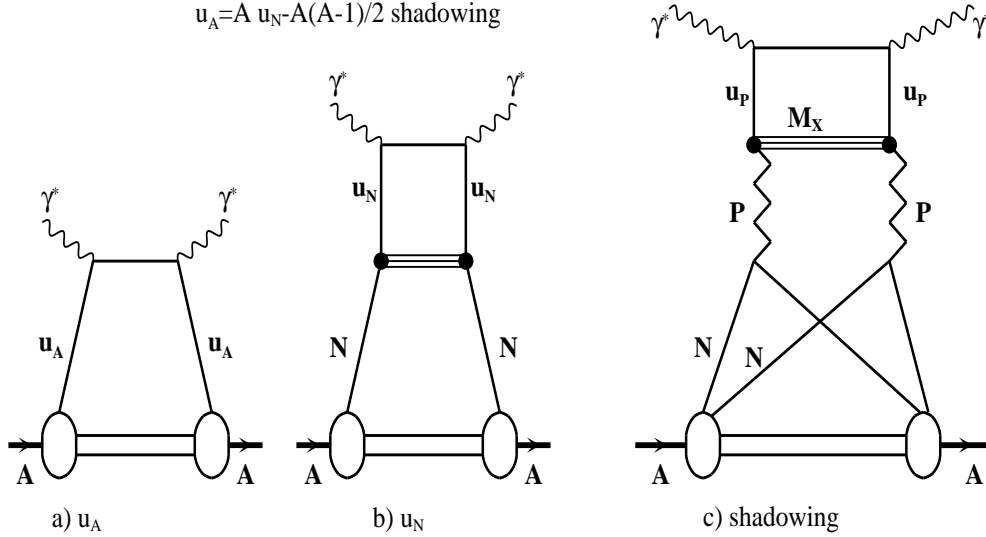


Figure 2: Feynman diagrams corresponding to Eq. (2.5) representing the nuclear quark distribution (a) as an incoherent sum of the quark distributions in the nucleons (b) minus the nuclear shadowing correction (c). Note that one needs to take the imaginary part of the forward amplitudes in order to find the structure functions.

However, Eq. (2.4) describes only one piece of the shadowing correction, namely the part which arises from the interaction with any two nucleons. Since the strength of the interaction with several nucleons is large, for a sufficiently heavy nucleus the interaction with three and more nucleons plays an important role. Such an interaction cannot be expressed directly in terms of diffraction on the nucleon and has to be modelled. We shall use a scheme inspired to a certain extent by the quasi-eikonal approximation, which successfully describes soft total hadronic cross sections of high energy hadron-nucleus interactions. In this approximation, the amplitude for the forward virtual photon-nucleus scattering is given by graphs containing virtual photon-nucleon cross sections of two kinds. These are the cross sections of diffractive scattering and the production of inelastic intermediate states, and cross sections of “elastic” rescattering of the produced inelastic states. In the formalism of cross section eigenstates [20], where one introduces the notion of a distribution of cross sections for the scattering state, the amplitude for the scattering off k nucleons is proportional to $\langle \sigma^k \rangle$ where $\langle \dots \rangle$ denotes averaging over the scattering state wavefunction. The quasi-eikonal approximation corresponds to the approximation

$$\frac{\langle \sigma^k \rangle}{\langle \sigma \rangle} = \sigma_{eff}^{k-1}. \quad (2.6)$$

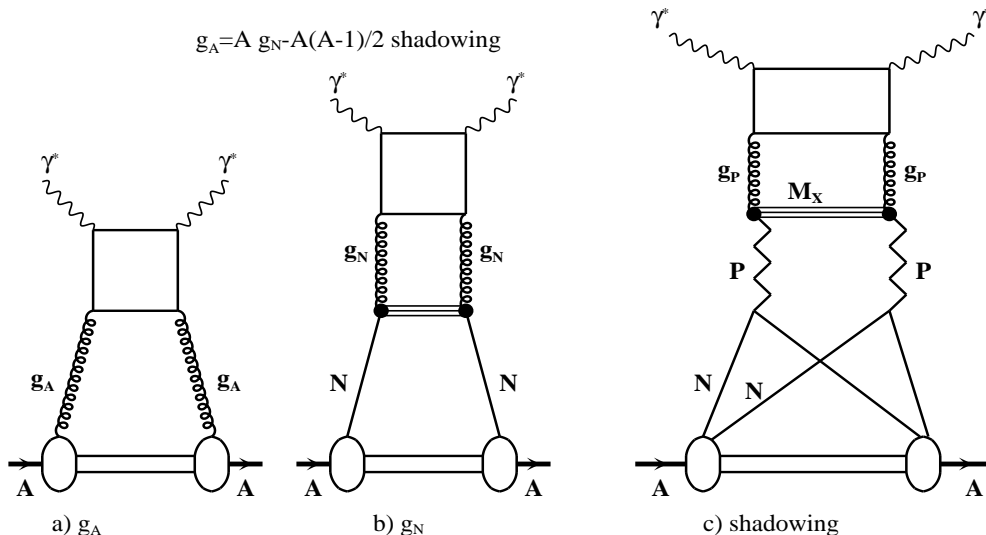


Figure 3: Feynman diagrams corresponding to Eq. (2.5) representing the nuclear gluon distribution (a) as an incoherent sum of the gluon distributions in the nucleons (b) minus the nuclear shadowing correction (c). Note that one needs to take the imaginary part of the forward amplitudes in order to find the structure functions.

One can interpret σ_{eff} as the average strength of the interaction of the produced configurations. In this approximation the total cross sections can be “eikonized” or summed to infinity in an exponential form in order to present the answer in a compact analytical expression (cf. [15]). Introducing the full nuclear shadowing correction to $f_{j/A}$, $\delta f_{j/A}$, where $\delta f_{j/A} = Af_{j/N} - f_{j/A}$, the quasi-eikonal approximation for $\delta f_{j/A}$ reads

$$\delta f_{j/A}(x, Q^2) = \frac{A(A-1)}{2} 16\pi \text{Re} \left[\frac{(1-i\eta)^2}{1+\eta^2} \int d^2b \int_{-\infty}^{\infty} dz_1 \int_{z_1}^{\infty} dz_2 \int_x^{x_{P,0}} dx_P \times \right. \\
 \left. f_{j/N}^D(\beta, Q^2, x_P, 0) \rho_A(b, z_1) \rho_A(b, z_2) e^{ix_P m_N (z_1 - z_2)} e^{-(A/2)(1-i\eta)\sigma_{eff}^j \int_{z_1}^{z_2} dz \rho_A(z)} \right]. \quad (2.7)$$

The rescattering cross section σ_{eff}^j is discussed further in appendix A.

Equation (2.7) implies that the rescattering cross section for the interaction with three and more nucleons, σ_{eff}^j , is the same as the rescattering cross section for the interaction with two nucleons. In general, this is not true since hadronic fluctuations with very different cross sections contribute to the total cross section of the interaction of a hard probe (virtual photon, W -boson, etc.) with a parton of the nucleus, and this broad dispersion over cross sections should be kept in mind. However, for nuclei with realistic finite A , numerical studies with models which include effects associated with the distribution over cross sections demonstrate that deviations from the quasi-eikonal approximation are small [21, 22]. Similar conclusions were reached in [23] for the case of nuclear shadowing, where an even broader range of possible cross section fluctuations was considered.

We used Eq. (2.7) in order to estimate $\delta f_{j/A}$ at some initial $Q^2 = Q_0^2$ ($Q_0^2 = 4 \text{ GeV}^2$ in our case). The result was used as an initial condition for the QCD evolution of $f_{j/A}$

to higher scales Q^2 . We would like to stress that it would be incorrect to apply Eq. (2.7) at any arbitrarily large Q^2 : as Q^2 increases, the QCD radiation of gluons and $q\bar{q}$ pairs increases the dispersion of cross section fluctuations and hence makes the quasi-eikonal approximation less justified.

2.1.2 The transition between shadowing and antishadowing: setting $x_{\mathcal{P},0}$.

The upper limit of integration over $x_{\mathcal{P}}$ in Eqs. (2.2, 2.4, 2.7), $x_{\mathcal{P},0}$, deserves a special discussion. In this subsection we motivate our choices for the numerical values of this parameter for the various parton species and explain that in our model this parameter effectively acts as the transition point from the shadowing region at low x to the antishadowing region at larger x . In [10], it was assumed that $x_{\mathcal{P},0} = 0.02$. This choice of $x_{\mathcal{P},0}$ was motivated by two observations. Firstly, only for $x_{\mathcal{P}} \leq 0.02$ is it valid to assume that the Pomeron contribution dominates diffraction, i.e., that sub-leading Reggeon exchanges can be safely neglected. Secondly, larger $x_{\mathcal{P},0}$ means that Eq. (2.4) can be applied to larger Bjorken x . However, for $x > 0.02$, nuclear parton distributions are expected to receive an additional contribution from nuclear antishadowing (the mechanism leading to the experimentally observed enhancement of nuclear inclusive structure functions), which is not included in Eq. (2.4). This makes the application of Eq. (2.4) for $x > 0.02$ not well motivated.

The HERA diffractive data indicate that Pomeron exchange dominates diffraction for $x_{\mathcal{P}} \leq 0.01$. At higher $x_{\mathcal{P}}$ it becomes necessary to take into account sub-leading Reggeon exchanges, although the ‘‘Pomeron term’’ appears to be giving the dominant contribution for $x_{\mathcal{P}} \leq 0.03$. At the same time the separation of the diffractive cross section into these two contributions in this kinematic region is definitely not unique and leads to some uncertainties. However, the sensitivity of the predictions resulting from Eq. (2.4) to the particular choice of $x_{\mathcal{P},0}$ is greatly reduced by the factor associated with the nuclear wavefunction, i.e., by the suppression factor $\rho_A(b, z_1)\rho_A(b, z_2)\exp(ix_{\mathcal{P}}m_N(z_1 - z_2))$.

Moreover, to perform a self consistent description of the parton densities for the whole range of x one needs to incorporate effects of enhancement of the parton densities at higher x . For the gluon such an enhancement follows from an energy-momentum sum rule analysis of the DIS nuclear data [24, 25] which revealed that the light-cone fraction carried by gluons in a nucleus and in a free nucleon is practically the same. For the valence quarks such an enhancement follows from the baryon charge sum rule [24]. For the antiquark/sea channel there are no general arguments to determine the effect of the enhancement and in fact no enhancement is observed in the Drell-Yan process⁷ [2]. Hence we followed a somewhat simplified scenario of [24, 25] which assumes that the enhancement is present only in the gluon and valence quark channels. The absence of the enhancement for the sea in principle allows one to take $x_{\mathcal{P},0}$ arbitrarily large. However, in our numerical analysis we set $x_{\mathcal{P},0} = 0.1$ for the sea. We explicitly checked that the answer is insensitive to the particular choice of $x_{\mathcal{P},0}$ due to the nuclear wavefunction suppression and the dominance of small- x values for the sea quark distributions.

⁷We note in passing that the observed pattern of the A -dependence of nuclear parton densities at $x \sim 0.1 - 0.2$ may be related to the origin of nuclear forces [24, 26].

We take $x_{\mathcal{P},0} = 0.03$ for the gluons. For the gluon case we need to introduce a transition from the shadowing to the antishadowing regions for some particular value of $x = x_{tr}$, which in general should depend on A . Arguments were given in [24] to the effect that the enhancement should be restricted to the region of $x < 0.2$, and could start somewhere in the range $x_{tr} \in [0.02, 0.05]$. In principle we could keep the same $x_{\mathcal{P},0} = 0.1$ as for the sea quarks and introduce an enhancement term for $x > x_{tr}$ to compensate for the shadowing term and to ensure an enhancement. As one can see from the structure of Eqs. (2.2, 2.4, 2.7), the shadowing correction vanishes when $x = x_{\mathcal{P},0}$, and is strongly suppressed close to it. Hence we find that for our numerical analysis it is simpler to take $x_{\mathcal{P},0} = x_{tr}$ and to neglect the enhancement term for $x \leq x_{tr}$.

The transition point between the shadowing and antishadowing regions for gluon distributions in nuclei has never been measured experimentally. The best one can do is to infer some information about x_{tr} for the gluons indirectly, using QCD evolution. Our choice of $x_{\mathcal{P},0}$ for the gluon distributions was motivated by the analysis in [26] of the NMC high statistics data on the ratio of structure functions F_2 of Tin (^{118}Sn) and Carbon (^{12}C) [27]. This analysis indicated that the transition between shadowing and antishadowing occurs for $0.023 \leq x \leq 0.035$ and $Q^2 \approx 4 \text{ GeV}^2$. Thus, we use $x_{\mathcal{P},0} = 0.03$ for the gluon distributions in our analysis. However, a choice of $x_{\mathcal{P},0}$ does not fix entirely the shape of the gluon distribution $g_A(x)$. We assumed a quadratic polynomial form for the antishadowing correction to $g_A(x)$ on the interval $0.03 \leq x \leq 0.2$. The three free coefficients of the quadratic fit were chosen such that the antishadowing correction vanishes at $x = 0.03$ and $x = 0.2$ and that the momentum fraction carried by gluons bound in nuclei is the same as that in the free nucleon [25]. A similar shape of the resulting gluon enhancement was assumed in [25, 28].

It is important to mention that, in this work, we make predictions for the shadowing corrections to the gluon and sea quark distributions in nuclei and do not concern ourselves with the valence quarks. In our numerical analysis, we keep only the Pomeron exchange contribution to $F_2^{D(4)}$, which has vacuum quantum numbers. Thus, nuclear shadowing for the valence quarks in nuclei, which is associated with the Reggeon exchanges with non-vacuum quantum numbers, is not considered and effects of the valence quark enhancement for $x \sim 0.1$ are neglected. In general, a complete model for the leading twist parton distributions in nuclei would require conservation of the baryon number and momentum sum rules [9] in order to reconstruct the nuclear enhancement of gluon and sea quark parton distributions at moderate x .

For the gluon and sea quark channels the corrections due to the A -dependence of the valence quark distributions (which are anyway rather small for the x -range we discuss) enter only through Q^2 -evolution and are very small, see e.g., [25, 28].

2.1.3 Numerical predictions for nuclear PDFs and F_2^A

In this subsection, we briefly discuss the DPDFs that we used in our analysis (we defer a more detailed specification to appendix A). We then present predictions for nuclear shadowing, both on the parton level (for both sea quarks and gluons) and for the nuclear structure functions, F_2^A , for a range of Q^2 and A .

High precision data on diffractive processes, taken at HERA, and their QCD analysis allow the diffractive parton distributions of the proton to be determined with good accuracy. In particular, both the ZEUS [29, 30, 31] and H1 [32] collaborations confirmed that a successful fit to the experimental data required a large gluon contribution (the same conclusion is drawn from an analysis based on the latest H1 data [33] on inclusive diffraction). One should especially note that the recent H1 data on diffractive photo- and electroproduction of dijets are dominated by the gluon diffractive structure functions [34]. We consider four different parameterizations of $f_{j/N}^D$: fit D of Alvero, Collins, Terron and Whitmore [17]; fit D of [17], which has been improved to include a low- β contribution; the parameterization from the theoretical light-cone model of Hautmann, Kunszt and Soper [35], and the H1 fit [18] to their own data [32]. Details of each of the parameterizations can be found in appendix A.

Predictions for nuclear parton distributions $f_{j/A}$ made with these parameterizations of $f_{j/N}^D$ are fairly consistent with each other. The spread of the predictions reflects the theoretical uncertainty in determining $f_{j/A}$ in terms of $f_{j/N}^D$ due to experimental errors, certain differences between H1 and ZEUS results, and the limited x and $x_{\mathbb{P}}$ ranges of the data. Furthermore, [17] did not include the most recent ZEUS and H1 data, while [35] actually did not perform a detailed fit to the data. In particular, the recent H1 data [33], which are most sensitive to the gluon diffractive structure functions, are best described by the H1 fits [18] to their earlier data, while the fit of Alvero *et al.* [17] somewhat overestimates the dijet production rate in the kinematics where the gluon DPDF at large β gives the dominant contribution⁸.

For nuclear shadowing of the gluon distribution in nuclei, there is also an important uncertainty associated with the unknown t -slope of the diffractive gluon distribution of the nucleon, $f_{g/N}^D$. A detailed analysis, presented in appendix A, demonstrates that Eqs. (2.2, 2.4, 2.7) require the diffractive parton distribution evaluated at $t \approx 0$. This implies that the answer for the shadowing correction is proportional to the t -slope of this distribution. The t -slope for the quark-dominated diffractive distributions in the proton, B_q , was measured in inclusive diffraction by ZEUS [30] to be $B_q = 7.2 \pm 1.1 \text{ GeV}^{-2}$ (see appendix A for explanations on our use of B_q). No experimental information about the t -slope of the gluon diffractive distribution, B_g , is available. In most of the phenomenological fits it is assumed that $B_g = B_q$. Since the amount of shadowing in the gluon channel increases with an increase of B_g (for fixed total gluon-induced diffraction) we take a conservative attitude and consider a minimum value for the slope, which originates solely from the coupling of a small object to a nucleon via two gluons. To estimate this *minimal* slope we used the recent data on the diffractive electroproduction of J/ψ by H1 [36] which can be parameterized in the following x -dependent form

$$B_g = \left(B_0 + 2\alpha'_{J/\psi} \ln(10^{-3}/x) \right) \text{ GeV}^{-2}, \quad (2.8)$$

⁸This is despite the fact that it has less shadowing. This effect is a peculiarity of the choices made by the various groups when choosing parameterizations for the input diffractive quark and gluon distributions in the regions of large ($\beta \sim 1$) and small β and reflects the residual uncertainties in the DPDFs. A larger DPDF at large β leads to a faster onset of nuclear shadowing at $x \sim 10^{-2}$, while the small- β region determines the amount of shadowing at $x \leq 10^{-4}$.

with $B_0 = 4.5 \text{ GeV}^{-2}$ and $\alpha'_{J/\psi} = 0.125 \text{ GeV}^{-2}$. The slow x -dependence describes an increase of the slope with increasing energy (“shrinkage”). In order to reflect the uncertainty associated with the slope B_g , we also considered a scenario of nuclear shadowing with $B_g = B_q$. For this choice, relative to that of Eq. (2.8), the shadowing of gluons, given by $1 - g_A/(Ag_N)$, increases by a factor of 1.6 at $x = 10^{-3}$, and of 1.4 at $x = 10^{-5}$, for light nuclei, and by a factor of 1.4 at $x = 10^{-3}$, and of 1.2 at $x = 10^{-5}$, for heavy nuclei.

It is important to note that all of the parameterizations of the gluon DPDF in the region of $x \sim 10^{-4} - 10^{-5}$ reach the unitarity limit for $Q^2 \sim 4 \text{ GeV}^2$ (see appendix A). This means that the probability of diffraction in gluon-induced DIS processes exceeds one half for these Q^2 . Hence, we are forced to tame the gluon DPDF at very small x in order to comply with the unitarity constraints. Note that, in the black-body limit, the cross section fluctuations are strongly suppressed: in principle reduces uncertainties in the predictions of shadowing for these x , within the framework of our calculation⁹.

Figs. 4 and 5 show our predictions for the ratio $f_{j/A}/(Af_{j/N})$ for the up-quark sea and gluon distributions, respectively, in a range of nuclei. They clearly illustrate that the effect of nuclear shadowing for gluons is larger than for the quarks, especially at the input scale $Q = 2 \text{ GeV}$. For instance, using the H1 parameterization, one finds at $Q = 2 \text{ GeV}$ and $x = 10^{-3}$ that the gluons are shadowed more than the quarks by a factor of 1.42 for ^{12}C and by a factor of 1.24 for ^{208}Pb . At $x = 10^{-5}$, due to the increase of B_q with energy and the unitarity taming of the gluon mentioned previously, shadowing for gluons and quarks are very similar. When the ACWT parameterization is employed, the gluons are shadowed more than the quarks by a factor of 1.70 for ^{12}C and by a factor of 1.39 for ^{208}Pb at $x = 10^{-3}$. At $x = 10^{-5}$, the factors are 1.29 for ^{12}C and 1.11 for ^{208}Pb .

Of the four parameterizations of diffractive parton distributions discussed in appendix A, we demonstrate only the two representative examples which give the largest (H1 [18]) and smallest (ACWT [17]) nuclear shadowing effects at $x = 10^{-5}$. This illustrates the spread of theoretical predictions for $f_{j/A}/(Af_{j/N})$ which arises from uncertainties in the diffractive parton distributions. The results are presented for $Q = 2 \text{ GeV}$ (solid curves), $Q = 5 \text{ GeV}$ (dashed curves) and $Q = 10 \text{ GeV}$ (dotted curves). At $Q = 2 \text{ GeV}$, Eq. (2.7) was used. For the inclusive parton distributions of the nucleon, the recent CTEQ5M parameterization [37] was employed. We used the nuclear PDFs, $f_{j/A}$, at $Q = 2 \text{ GeV}$ as input to the DGLAP evolution equations in order to find $f_{j/A}$ at $Q = 5, 10 \text{ GeV}$.

One can see from the figures that differences between the predictions are large for $x \sim 0.01$, where contribution of the large $\beta \gtrsim 0.3 - 0.6$ region dominates. This β region was not strongly constrained by the older data from which the fits are derived.

For the region of $x \sim 10^{-3}$ predictions for sea quark shadowing exhibit minimal spread because the integrals over $x_{\mathbb{P}}$ in Eq. (2.7) are dominated by regions where the diffractive data is of high precision. The spread of predictions increases again for $x \leq 10^{-4}$ reflecting the extrapolation of the DPDFs to the region of very high energies (beyond the HERA range). In the gluon case the spread is even larger, reflecting greater uncertainties in extraction of gluon diffractive distributions from the scaling violation of the $F_2^{D(3)}$ data.

⁹However, since the approach to this limit is not understood and must involve new effects, our confidence in the predictions decreases.

Of two parameterizations presented here, only the H1 parameterization fits the dijet data, which indicates that it may be more realistic.

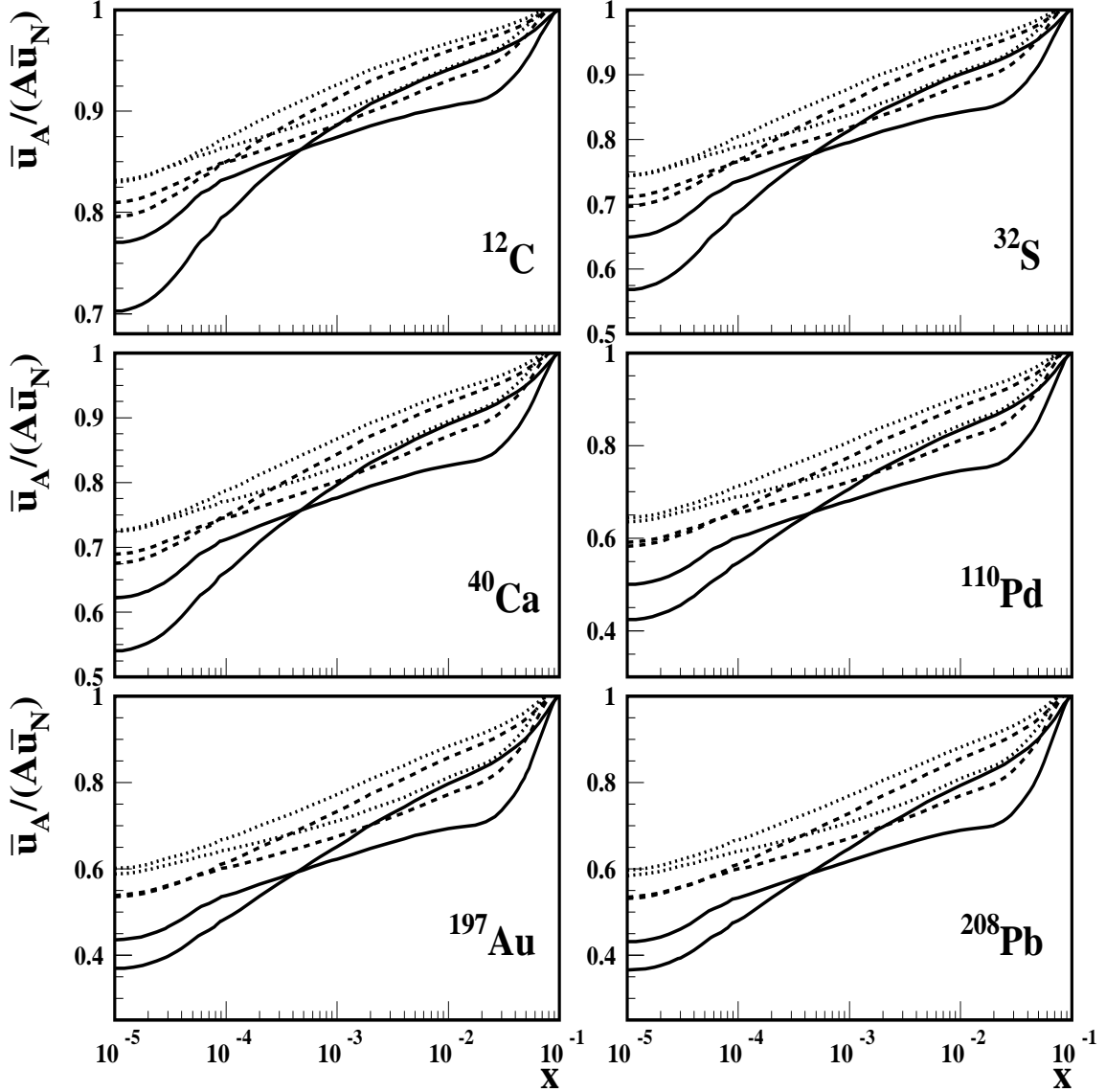


Figure 4: The ratio of nuclear to nucleon sea up-quark distributions, $\bar{u}_A/(A\bar{u}_N)$, at $Q = 2$ GeV (solid line), $Q = 5$ GeV (dashed line), and $Q = 10$ GeV (dotted line). For each case, the scenarios with the largest (based on [18]) and smallest (based on [17]) nuclear shadowing for $x = 10^{-4}$ are presented.

It was observed in [10] that shadowing for gluons, calculated using the DPDFs of Alvero *et al.* [17], is much larger than for the sea quarks. The present analysis demonstrates that this is quite sensitive to the particular choice of the input diffractive parton distribution functions. However, it would appear from Figs. 4 and 5 that for the smallest x values nuclear shadowing for sea quarks is not so much different from that for the gluons. There are several reasons for this. Firstly, and most importantly, our numerical calculations

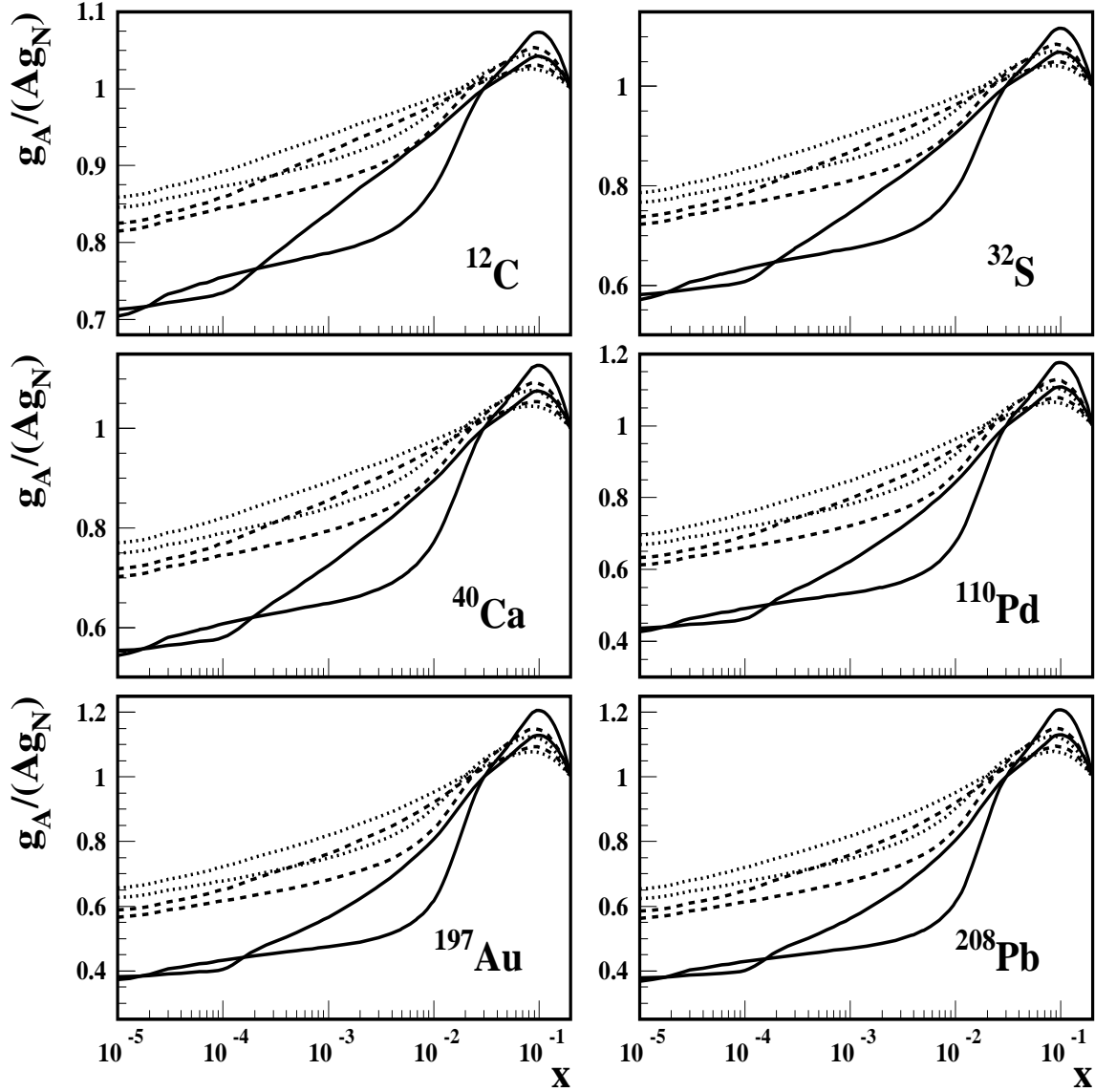


Figure 5: The ratio of nuclear to nucleon gluon distributions, $g_A/(Ag_N)$ at $Q = 2$ GeV (solid line), $Q = 5$ GeV (dashed line), and $Q = 10$ GeV (dotted line). For each case, the scenarios with the largest (based on [18]) and smallest (based on [17]) nuclear shadowing for $x = 10^{-4}$ are presented.

were performed using the slope B_g , given by Eq. (2.8), which is smaller than $B_g = B_q$, as implemented in [10]. Secondly, the effective cross section for the gluon channel, σ_{eff}^g , which defines the size of nuclear shadowing in Eqs. (2.2) and (2.4) for gluons, cannot be too large, otherwise the diffractive cross section becomes larger than allowed by unitarity of the scattering operator. Thus, in our model shadowing for the gluons reaches a plateau at $Q \sim 2$ GeV for $x < 10^{-4}$, when the H1 parameterization is used. In case of the ACWT fit, no taming of σ_{eff}^g is necessary down to $x = 10^{-5}$. This shows that it is impossible to make realistic calculations of nuclear shadowing at small enough x, Q without invoking the unitarity restrictions. Also, the reverse statement is true: estimates of the kinematical

boundaries of the region in which unitarity restrictions play a role require that nuclear shadowing effects be properly taken into account!

In order to demonstrate the importance of the value of B_g , we also performed an analysis with larger B_g : $B_g = B_q$. The results are presented in Fig. 6 for the lightest (^{12}C) and heaviest (^{208}Pb) nuclei, using the H1 DPDF. The thin curves are those from Fig. 5 (using B_g from Eq. (2.8)), while the thick curves are obtained using $B_g = B_q$. Again, the solid, dashed and dotted curves correspond to $Q = 2, 5, 10$ GeV. One observes that increasing the t -slope of the gluon DPDF increases the shadowing correction to g_A , given by $1 - g_A/(Ag_N)$. For example, at $x = 10^{-3}$ and $Q = 2, 5, 10$ GeV, $1 - g_A/(Ag_N)$ increases by 60% for ^{12}C and 40% for ^{208}Pb . At $x = 10^{-5}$, the increase is about 40% for ^{12}C and 20% for ^{208}Pb .

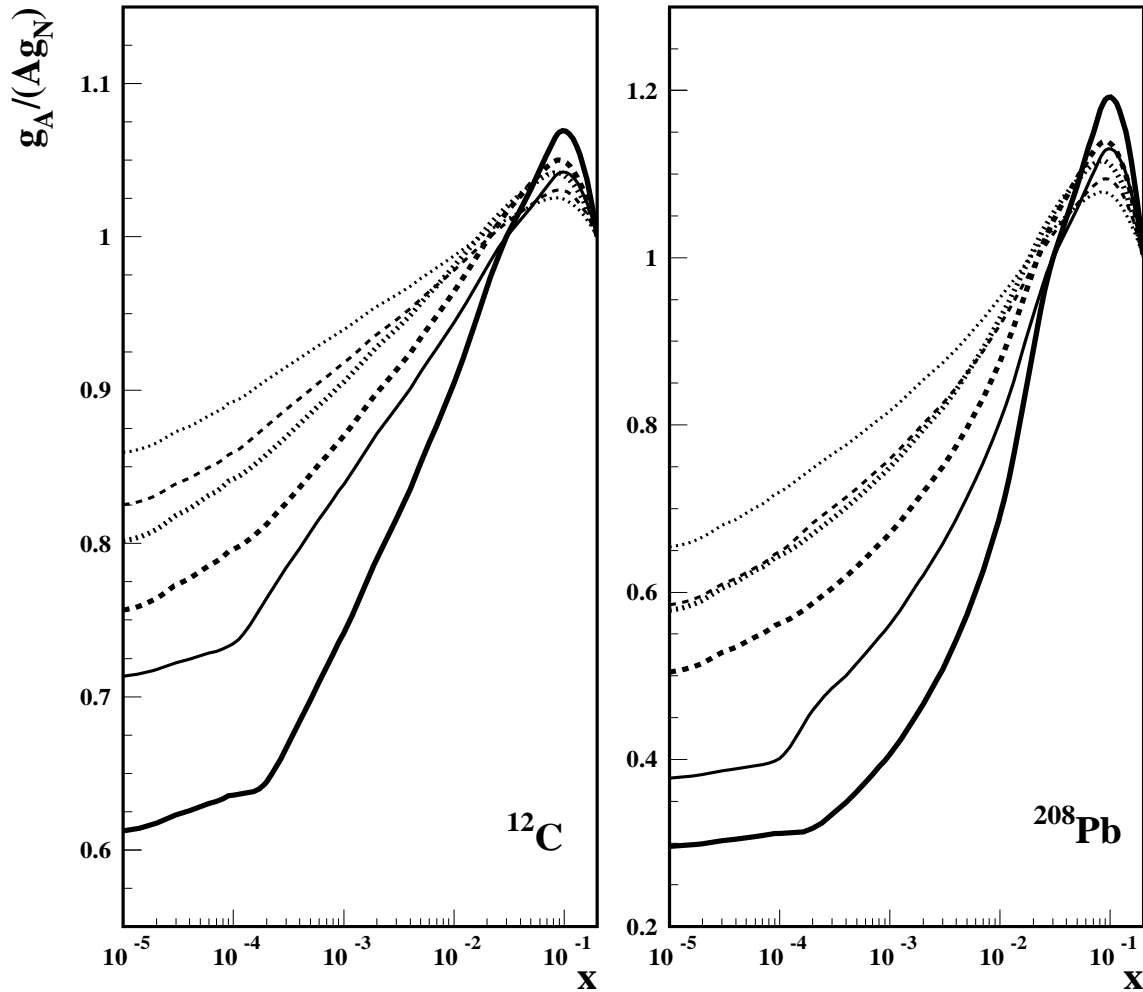


Figure 6: The ratio of nuclear to nucleon gluon distributions, $g_A/(Ag_N)$ at $Q = 2$ GeV (solid line), $Q = 5$ GeV (dashed line), and $Q = 10$ GeV (dotted line). The H1 parameterization [18] for diffractive parton distributions is employed. The thin curves correspond to B_g of Eq. (2.8), the thick curves correspond to $B_g = B_q$.

Using our results for the sea quark ratio $\bar{q}_A/(A\bar{q}_N)$ and the gluon ratio $g_A/(Ag_N)$, one

can readily predict the ratio of the inclusive structure functions $F_2^A/(AF_2^N)$. In next to leading order accuracy, F_2^A can be presented in the standard form [38]

$$F_2^A(x, Q^2) = \sum_i e_i^2 (q_A^i(x, Q^2) + \bar{q}_A^i(x, Q^2)) \quad (2.9)$$

$$+ \frac{\alpha_s(Q^2)}{2\pi} x \int_x^1 \frac{dy}{y} \left[C_2^q(x/y) \sum_i e_i^2 (q_A^i(y, Q^2) + \bar{q}_A^i(y, Q^2)) + \langle e^2 \rangle C_2^g(x/y) g_A(y, Q^2) \right].$$

Here e_i is the electric charge of the quark with flavor i ; $\langle e^2 \rangle = (\sum_i e_i^2)/n_f$; C_2^q and C_2^g are the target-independent hard scattering coefficients

$$C_2^q = \frac{4}{3} \left[\frac{1+x^2}{1-x} \left(\ln\left(\frac{1-x}{x}\right) - \frac{3}{4} \right) + \frac{1}{4}(9+5x) \right]_+,$$

$$C_2^g = n_f \left((x^2 + (1-x)^2) \ln\left(\frac{1-x}{x}\right) - 1 + 8x(1-x) \right), \quad (2.10)$$

where n_f is the number of active quark flavors and $[\dots]_+$ denotes the plus-regularization. In our analysis, $n_f = 4$. In order to obtain F_2^N , one needs to replace the nuclear parton distributions by the nucleon ones in Eq. (2.9).

We considered two scenarios of nuclear shadowing, corresponding to ACWT and H1 parameterizations of DPDFs. In the former case, since the DPDFs of the strange quarks is zero at the initial scale $Q_0 = 2$ GeV, only up and down quarks and gluons are shadowed at the initial scale. However, when the H1 parameterization is used, $f_{u/N}^D = f_{d/N}^D = f_{s/N}^D$ at the initial scale so that up, down and strange quarks are shadowed. For both of the parameterizations of DPDFs we considered, the charm quarks are not affected by the nuclear medium at the initial scale, i.e., $c_A = Ac_N$. However, as a result of the QCD evolution, gluons convert into $s\bar{s}$ and $c\bar{c}$ pairs, which leads to a significant deviation of the ratios $s_A/(As_N)$ and $c_A/(Ac_N)$ from unity (see Fig. 9).

The results of the calculation using Eq. (2.9) are presented in Fig. 7. In this analysis we assumed that valence quarks are shadowed the same as the sea quarks. A comparison of Figs. 4 and 7 reveals that while at $Q = 5, 10$ GeV, the ratios $\bar{u}_A/(A\bar{u}_N)$ and $F_2^A/(AF_2^N)$ are quite similar, $F_2^A/(AF_2^N)$ is smaller than $\bar{u}_A/(A\bar{u}_N)$ at $Q = 2$ GeV due to the important contribution of the unshadowed charm quarks.

One can see from Fig. 7 that the solid curves corresponding to $Q = 2$ GeV run close to each other between $x = 10^{-4}$ and $x = 10^{-2}$. In order to understand this pattern, one should recall Eq. (2.7) which demonstrates that δF_2^A is linearly proportional to $F_2^{D(4)}$ in the low nuclear density limit. Since both the ACWT and H1 parametrizations give a good fit to $F_2^{D(4)}$, it is no surprise that the resulting shadowing corrections to F_2^A in the appropriate range of x are virtually the same for both fits.

A peculiar feature of Fig. 7 is that the upper solid curves, which correspond to the calculation with the ACWT DPDF at $Q = 2$ GeV, in the small- x region lie above (i.e., correspond to smaller nuclear shadowing) all other curves corresponding to higher Q^2 . There are two reasons for this. Firstly and most importantly, the absence of nuclear shadowing for charm quarks at the initial scale significantly decreases the nuclear shadowing correction to F_2^A . Secondly, the next to leading order contribution to F_2^A (terms proportional to $\alpha_s(Q^2)$ in Eq. (2.9)) has reduced shadowing as a result of the integration over y .

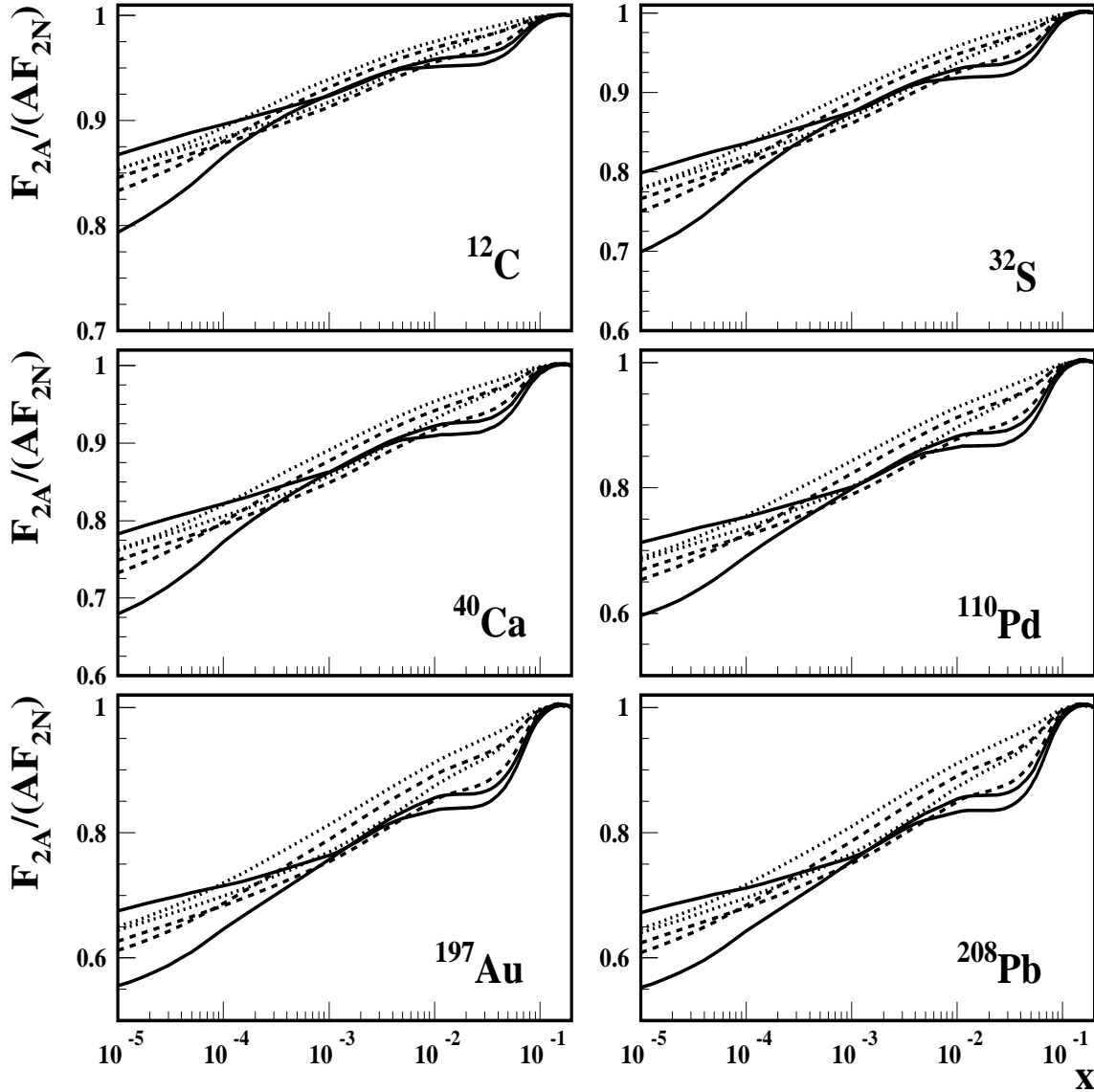


Figure 7: The ratio of nuclear to nucleon inclusive structure functions $F_2^A/(AF_2^N)$. The solid, dashed and dotted curves correspond to $Q = 2, 5, 10$ GeV and the scenarios of nuclear shadowing are as in Fig. 4.

We would like to point out that there is no reason to assume that nuclear shadowing for the charm quarks is zero at the initial evolution scale. We propose the following simple model. At small values of Bjorken x charm quarks are mostly produced by QCD evolution because of the splitting $g \rightarrow c\bar{c}$. Thus, nuclear shadowing for the charm quarks at some x and $Q = Q_0$ originates from nuclear shadowing of gluons at larger x and Q_{eff} . We choose

$$\frac{c_A(x, Q_0^2)}{Ac_N(x, Q_0^2)} = \frac{g_A(2x, Q_{eff}^2)}{Ag_N(2x, Q_{eff}^2)}, \quad (2.11)$$

where $Q_{eff}^2 = 4m_c^2 + Q_0^2 = 11 \text{ GeV}^2$. Note that the gluon distributions are taken at twice the x -values of the charm quarks.

With this model for nuclear shadowing for charm quarks we re-evaluated the ratio $F_2^A/(AF_2^N)$ using the H1 parametrization of DPDFs. The results are presented in Fig. 8 as thin curves and compared to the corresponding curves from Fig. 7 (thick curves). One can see that by introducing nuclear shadowing for the charm quarks at the initial scale by Eq. (2.11), one increases nuclear shadowing correction to F_2^A and makes it closer to the shadowing correction to \bar{u}_A . However, the size of nuclear shadowing introduced by our physically motivated model of Eq. (2.11) is not sufficient to have $F_2^A/(AF_2^N) \approx \bar{u}_A/(Au_N)$ at small x .

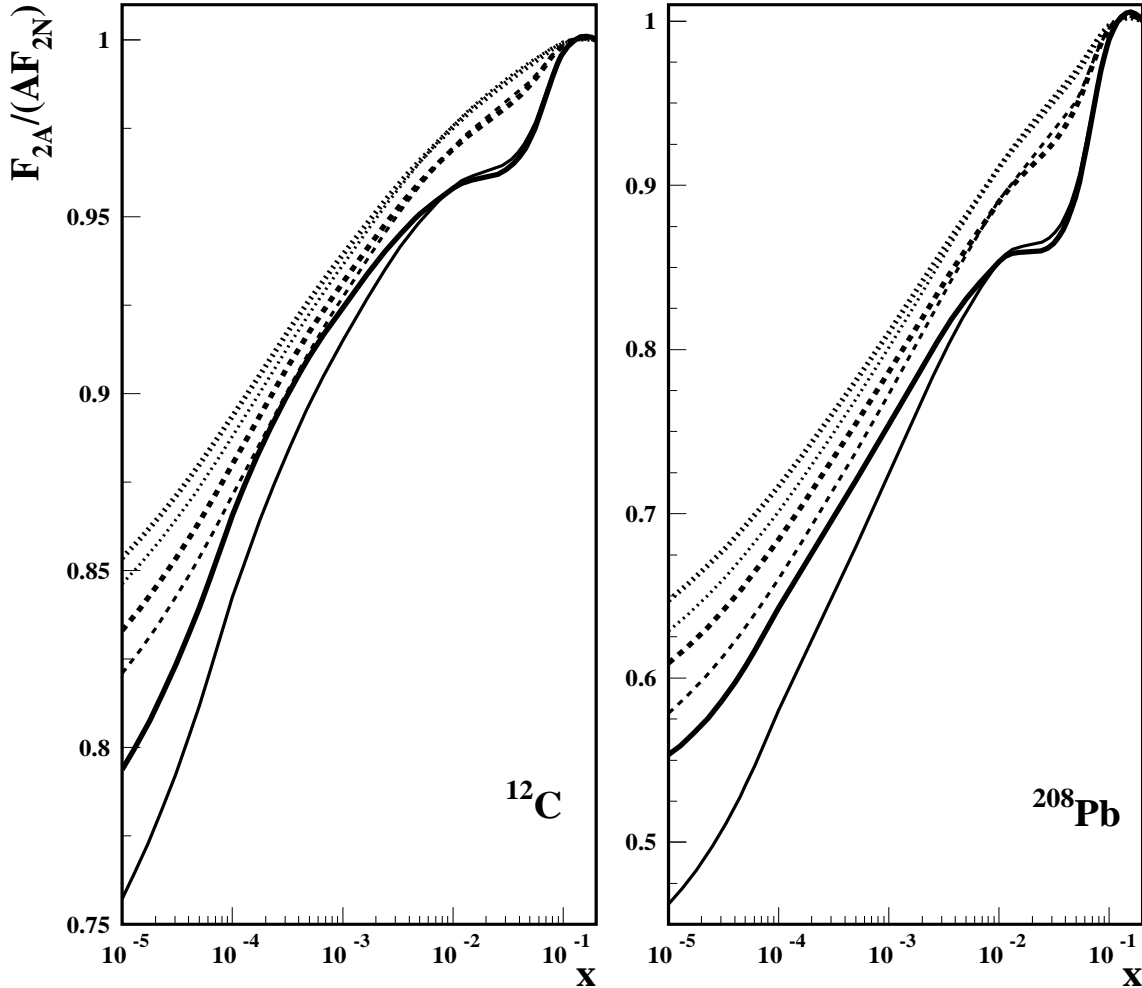


Figure 8: The ratio of nuclear to nucleon inclusive structure functions $F_2^A/(AF_2^N)$. The thick curves are those from Fig. 7, while the thin ones correspond to the calculation with shadowing for the charm quarks given by Eq. (2.11) at the initial scale $Q = 2$ GeV. The calculation is done using the H1 parametrization of DPDFs.

Both scenarios of nuclear shadowing for charm quarks at $Q = 2$ GeV and the results of their QCD evolution are presented in Fig. 9 using the H1 fit to DPDFs. The thick curves represent our standard scenario without shadowing for the charm quarks at the initial scale, while the thin curves correspond to the calculation with shadowing for the charm quarks,

see Eq. (2.11). The Q^2 -dependence of the curves is the same as in Fig. 4. Two features of Fig. 9 are of interest: significant antishadowing and “wrong” Q^2 dependence of nuclear shadowing – nuclear shadowing increases as Q^2 increases! Both of these features can be understood as a consequence of the fact that at low x , charm quarks are predominantly produced by photon-gluon fusion $\gamma^*g \rightarrow c\bar{c}$.

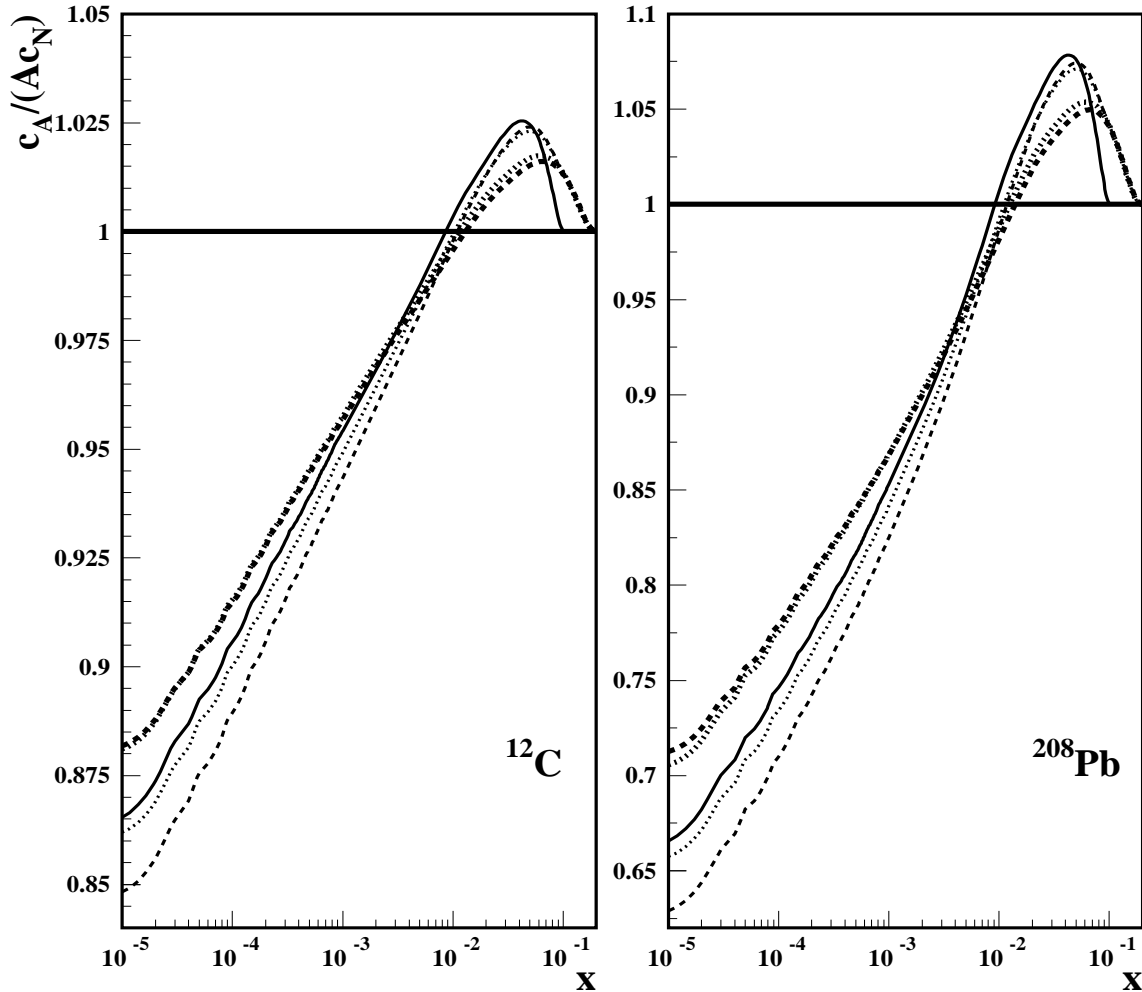


Figure 9: The ratio of nuclear to nucleon charm distribution functions, $c_A/(Ac_N)$. The solid, dashed and dotted curves correspond to $Q = 2, 5, 10$ GeV and the scenarios of nuclear shadowing are as in Fig. 4. The calculation is done using the H1 parametrization of DPDFs.

The consistent inclusion of heavy quarks in input boundary conditions and in QCD evolution is known to be highly non-trivial, and involves a certain dependence on the scheme one is using for the number of active quark flavours (see [39] and references therein). This is one reason why such a low starting scale (i.e., below the charm mass) is often chosen, e.g., by CTEQ, so that heavy quarks are only generated explicitly via photon-gluon fusion at the input scale. Taken literally this implies that there can be no shadowing of charm at the input scale since there is no intrinsic charm at this scale! We attempt to correct for this, in a phenomenological way, by using Eq. (2.11) above. However, a more accurate

treatment, along the lines of variable flavour number scheme, would be desirable but is beyond the scope of this paper.

2.1.4 Predictions for central collisions

The effect of nuclear shadowing becomes even more dramatic if one considers DIS from nuclei at small impact parameters (i.e., “central” collisions). In this case, since the density of nucleons is larger in the centre of the nucleus than at its periphery, the number of scatterers effectively increases, which leads to an increase of nuclear shadowing. Experimentally, one can tag such small impact parameter events by measuring slow “knock-out” neutrons [40] which, in collider experiments with symmetric beam energies, can be detected with a very high efficiency ($\sim 100\%$) by low angle neutron calorimeters.

Let us introduce a simple model for impact parameter-dependent nuclear PDFs, $f_{j/A}(x, Q^2, b^2)$. By our definition, $f_{j/A}(x, Q^2, b^2)$ are simply related to the usual, or impact parameter integrated parton distributions, $f_{j/A}(x, Q^2)$, via

$$\int d^2b f_{j/A}(x, Q^2, b^2) = f_{j/A}(x, Q^2) . \quad (2.12)$$

In common with $f_{j/A}(x, Q^2)$, $f_{j/A}(x, Q^2, b^2)$ can be presented as a difference between the impulse approximation and shadowing contributions:

$$f_{j/A}(x, Q^2, b^2) = \left(\int_{-\infty}^{\infty} dz \rho_A(b, z) \right) A f_{j/N}(x, Q^2) - \delta f_{j/A}(x, Q^2, b^2) . \quad (2.13)$$

Here the factor $\int_{-\infty}^{\infty} dz \rho_A(b, z)$ guarantees the correct normalization of $f_{j/A}(x, Q^2, b^2)$ (see Eq. (2.12)). The shadowing correction $\delta f_{j/A}(x, Q^2, b^2)$ can be readily found from Eq. (2.7) by removing the integration over b :

$$\delta f_{j/A}(x, Q^2, b^2) = \frac{A(A-1)}{2} 16\pi \text{Re} \left[\frac{(1-i\eta)^2}{1+\eta^2} \int_{-\infty}^{\infty} dz_1 \int_{z_1}^{\infty} dz_2 \int_x^{x_{\mathcal{P},0}} dx_{\mathcal{P}} \times \right. \\ \left. f_{j/N}^D(\beta, Q^2, x_{\mathcal{P}}, 0) \rho_A(b, z_1) \rho_A(b, z_2) e^{ix_{\mathcal{P}} m_N (z_1 - z_2)} e^{-(A/2)(1-i\eta)\sigma_{eff}^j \int_{z_1}^{z_2} dz \rho_A(z)} \right] \quad (2.14)$$

We used Eq. (2.14) in exactly the same way that we used Eq. (2.7). Firstly, the nuclear shadowing correction to the gluon and sea quark parton impact parameter-dependent parton distributions was evaluated using Eq. (2.14) at the initial scale $Q_0 = 2$ GeV. Secondly, antishadowing was modelled so that gluons in nuclei carry the same momentum per nucleon as in the free nucleon. Thirdly, the shadowing and antishadowing calculations defined the input to the QCD evolution to higher Q^2 scales. The results of such an analysis for the gluon distributions at the zero impact parameter are presented in terms of the ratio $g_A(x, Q^2, b=0)/(AT(0)g_N)$ in Fig. 10 ($T(0) = \int dz \rho_A(b=0, z)$). The deviation of this ratio from unity is an effect of nuclear shadowing at small x and antishadowing for $0.03 < x < 0.2$. The results of Fig. 10 should be compared with those of Fig. 5. By selecting DIS events with low impact parameters one can significantly increase nuclear shadowing. For instance, for $Q = 2, 5, 10$ GeV and $x = 10^{-3}$ and $x = 10^{-5}$, the increase is about 55 – 75% for ^{12}C and 20 – 40% for ^{208}Pb .

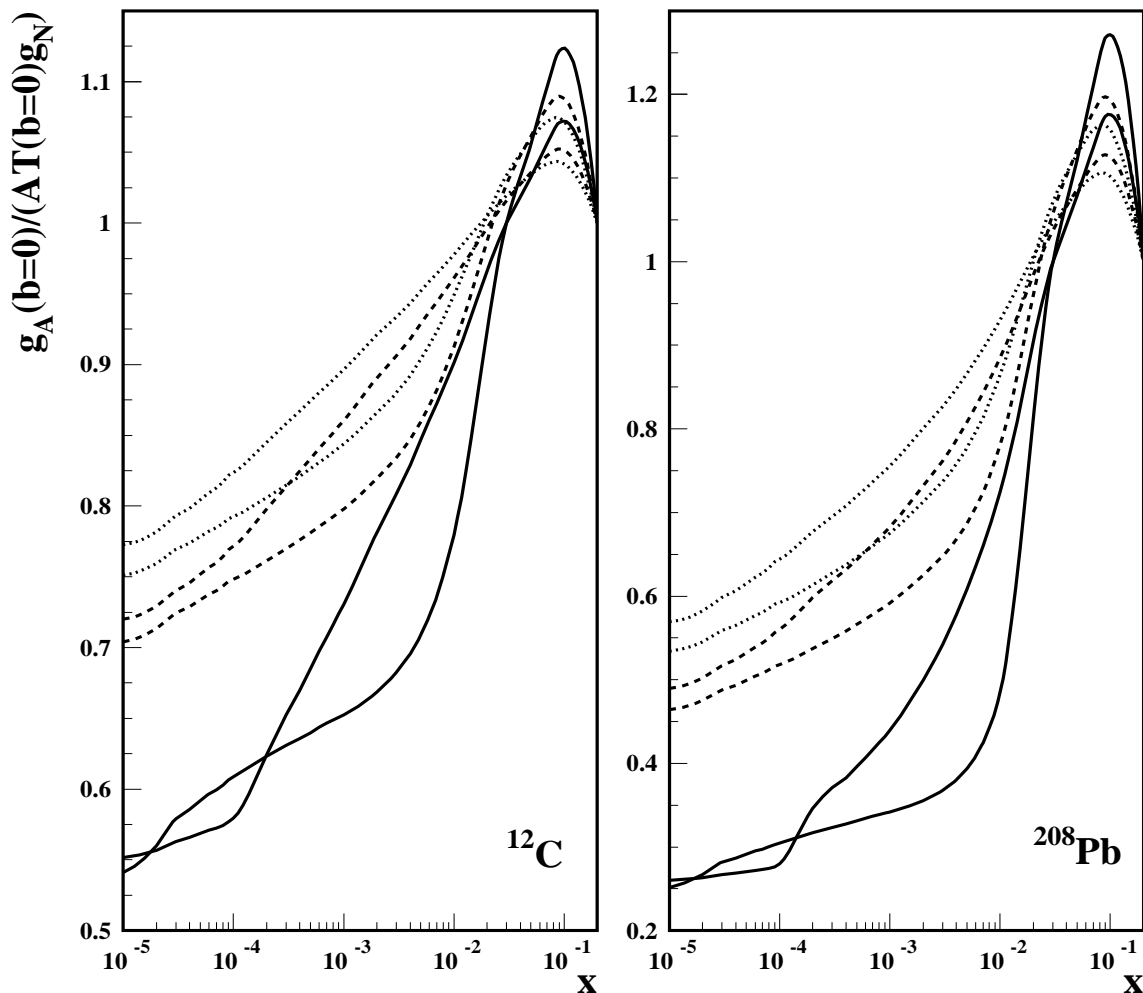


Figure 10: The ratio of the nuclear gluon distribution at the zero impact parameter to that of the nucleon, $g_A(x, Q^2, b=0)/(AT(0)g_N)$ at $Q = 2$ GeV (solid line), $Q = 5$ GeV (dashed line), and $Q = 10$ GeV (dotted line). The ACWT [17] and H1 [18] parameterizations for diffractive parton distributions are employed.

2.2 The eikonal approximation approach

Another popular and frequently used approach to nuclear shadowing is the eikonal approximation. The essence of this method in DIS on nuclei is the assumption that the forward amplitude for the virtual photon interaction with a nucleus can be written as the probability of the transition $\gamma^* \rightarrow q\bar{q}$ (the virtual photon light-cone wavefunction) convoluted with an *exponential* factor describing the interaction of the $q\bar{q}$ pair with the nucleons of the nucleus. The exponential factor is obtained by summing an infinite series of terms proportional to powers of the total $q\bar{q}$ -nucleon scattering cross section (i.e., by *eikonalizing*, hence the name of the approximation).

An eikonalized form for high energy scattering amplitudes was first obtained by Cheng and Wu [41], for several processes in QED. In particular, these authors demonstrated that for processes such as Delbruck scattering (photon-nucleus scattering in the static

approximation) the sum of Feynman graphs of a certain type can be cast in the form of a convolution of the e^+e^- -component of the virtual photon wavefunction with the eikonized amplitude for the e^+e^- -nucleon scattering.

Two aspects of the QED derivation of [41] are important to mention. Firstly, it was explicitly demonstrated that higher order diagrams, involving closed electron loops or graphs, in which a photon is allowed to be emitted and absorbed by the same electron, do not exponentiate. Secondly, the transverse diameter of the e^+e^- -system emitted by the photon remains unchanged by the interaction.

At ultra-relativistic energies, the eikonal approximation has been successful in the description of hadron-hadron scattering (for instance, the droplet model of [42]) as well as hadron-nucleus scattering (see, for example, [43] and [44]). The approximation can be also applied to nucleus-nucleus scattering at high energies.

The use of the eikonal approximation in high energy DIS on nuclei, within a dipole model for the wavefunction of a virtual photon, constitutes an extension of its previous use in hadron-nucleus scattering and QED. As explained above, the forward virtual photon-nucleus amplitude is given by the square of the photon light-cone wavefunction multiplied by an eikonal factor arising from the exponentiation of the *total* $q\bar{q}$ -nucleon scattering cross section. Such a form is based on the strong assumption that the $q\bar{q}$ -nucleon interaction leaves certain characteristics of the $q\bar{q}$ -system, such as its transverse diameter and momentum fraction sharing variable, unchanged, i.e., the interaction is diagonal in the appropriate variables. In other words, within the eikonal approximation the projectile is said to be frozen in its prepared state for the lifetime of the interaction.

A diagram typical of the eikonal approximation, as applied to nuclear shadowing, is shown in Fig. 11. It represents the imaginary part of the forward virtual photon-nucleus scattering amplitude, in which the interaction with only a pair of nucleons is taken into account. Such a graph gives rise to the shadowing correction, $\delta F_2^{A(2)}$, and should be compared to Fig. 1 of the leading twist approach. The differences between the two figures reveal conceptual differences between the approaches: while in Fig 1 the virtual photon interacts by dissociating into a multitude of diffractive intermediate states, the $q\bar{q}$ -dipole of the virtual photon in Fig. 11 interacts elastically through the exchange of an interacting gluon ladder (illustrated by the exchange of two gluons).

In quantum mechanical processes, and high-energy hadron-nucleus scattering, the approximation that the dominant fluctuations of the projectile can be considered to be frozen, can be justified by a suitable choice of basis states which diagonalize the scattering operator. However, this is not the case in QCD, where we are already given the basis, i.e., the quark and gluon degrees of freedom. In QCD, the $q\bar{q}$ -fluctuation of the virtual photon necessarily emits gluons, which can emit further partons, etc. The Fock components of the virtual photon, $|q\bar{q}\rangle$, $|q\bar{q}g\rangle$, \dots , intermingle before and during the interaction with the target, i.e., those states are not eigenstates of the scattering operator and cannot in general be considered to be frozen. Intuitively, the observation that emitting extra gluons would lead to the breakdown of the eikonal approximation is similar to the finding of [41] that the graphs where a photon is emitted and absorbed by the same fermion line, do not eikonize.

Since the eikonal approximation is so successful in describing cross sections of nucleon-

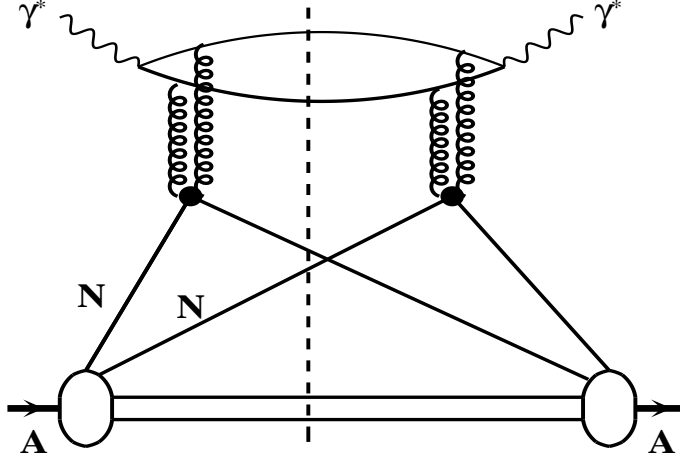


Figure 11: Feynman diagram giving rise to nuclear shadowing within the eikonal approximation.

nucleus scattering, should it not also be a good method to describe lepton-nucleus DIS? The above discussion shows that the eikonal approximation is justified only for processes where the presence of the $|q\bar{q}g\rangle$ -component of the virtual photon is unimportant. An example of a relevant observable is F_2^A at Q^2 of only a few GeV^2 . On the other hand, for reactions sensitive to the $|q\bar{q}g\rangle$ -component, the eikonal approximation is expected to fail and give wrong size and Q^2 -dependence of nuclear shadowing. One example of an observable for which this effect is dramatic is the longitudinal structure function F_L^A .

Within the eikonal approximation, the shadowing correction to the nuclear inclusive structure function F_2^A , δF_2^A , can be written in the form [15]

$$\begin{aligned} \delta F_2^A(x, Q^2) = & \frac{Q^2}{4\pi^2\alpha_{em}} \text{Re} \left[\int d\alpha d^2d_t \sum_i |\Psi(\alpha, Q^2, d_t^2, m_i)|^2 \frac{A(A-1)}{2} \times \right. \\ & \int d^2b \int_{-\infty}^{\infty} dz_1 \int_{z_1}^{\infty} dz_2 (1-i\eta)^2 \left[\sigma_{q\bar{q}N}^{\text{tot}}(x, d_{\perp}^2, m_i) \right]^2 \rho_A(b, z_1) \rho_A(b, z_2) e^{i2xm_N(z_1-z_2)} \times \\ & \left. e^{-(A/2)(1-i\eta)\sigma_{q\bar{q}N}^{\text{tot}}(x, d_{\perp}^2, m_i) \int_{z_1}^{z_2} dz \rho_A(z)} \right]. \end{aligned} \quad (2.15)$$

Here α_{em} is the fine-structure constant; α is the fraction of the photon's longitudinal momentum carried by q or \bar{q} ; d_t is the transverse diameter of the $q\bar{q}$ -system; m_i is the mass of the quark with flavor i ; ρ_A is the nuclear one-body density. The square of the light-cone wavefunctions of the virtual photon is given by the standard expression

$$\begin{aligned} |\Psi(\alpha, Q^2, d_t^2, m_i)|^2 = & \frac{6\alpha_{em}}{\pi^2} \sum_i e_i^2 \left[\left(Q^2\alpha^2(1-\alpha)^2 + \frac{m_i^2}{4} \right) K_0^2(\epsilon_i d_t) \right. \\ & \left. + \frac{1}{4} \left(\alpha^2 + (1-\alpha)^2 \right) \epsilon_i^2 K_1^2(\epsilon_i d_t) \right], \end{aligned} \quad (2.16)$$

where K_0 and K_1 are the modified Hankel functions; $\epsilon_i = Q^2\alpha(1-\alpha) + m_i^2$; η is the ratio of the real to imaginary parts of $q\bar{q}$ -nucleon scattering amplitude. In our analysis, we set

$\eta = 0.25$, which is consistent both with our leading twist calculations and vector meson dominance ideas, see e.g., [15]. Note that since F_2 measures the virtual photon-target cross section averaged over helicities of the incoming photon, averaging over the photon helicities is assumed in Eqs. (2.15) and (2.16). Following our analysis in [45], we include four flavors of quarks and assume $m_u = m_d = m_s = 300$ MeV and $m_c = 1.5$ GeV.

The use of the optical theorem for the elementary $q\bar{q}$ -nucleon amplitudes enables one to express the answer in Eq. (2.15) through the total $q\bar{q}$ -nucleon cross section, $\sigma_{q\bar{q}N}^{tot}$. This cross section plays a key role in the so-called dipole formalism of DIS, and we refer the reader to [46] for a brief review of various formulations of the dipole formalism existing in the literature. In this analysis, we used a QCD-motivated model for $\sigma_{q\bar{q}N}^{tot}$ developed in [45]. For small dipoles, the total cross section is predominantly inelastic and, as such, is governed by the gluon distribution in the proton. In the non-perturbative region of large dipole sizes, we model $\sigma_{q\bar{q}N}^{tot}$ by requiring its equivalence to the soft pion-nucleon total cross section.

In exactly the same or very similar form, Eq. (2.15) was used in a number of papers [47, 48, 49, 50, 51, 52]. In the derivation of Eq. (2.15) one assumes that the invariant mass of all $q\bar{q}$ -dipole intermediate states, which is inversely proportional to the dipole diameter d_t , is the same and approximately equal to Q (i.e., the diffractive variable $\beta = Q^2/(Q^2 + M^2) \approx 0.5$, which implies $x_P \approx 2x$). This means that the non-zero longitudinal momentum transfer to each individual nucleon of the nuclear target is of the order of $2xm_N$, which explains the factor $\exp(i2xm_N(z_1 - z_2))$ in Eq. (2.15).

We would like to stress the following subtle point, which should be kept in mind while applying Eq. (2.15) and which was ignored in [48, 49, 50, 51, 52]. The total cross section $\sigma_{q\bar{q}N}^{tot}$ receives contributions from both elastic, $\sigma_{q\bar{q}N}^{el}$, and inelastic, $\sigma_{q\bar{q}N}^{inel}$, cross sections. For small dipole sizes and not very small x , $\sigma_{q\bar{q}N}^{inel}$ is relatively small and can be calculated using methods of perturbative QCD. Moreover, in this case $\sigma_{q\bar{q}N}^{el}$ is negligibly small and thus one can identify $\sigma_{q\bar{q}N}^{tot}$ with $\sigma_{q\bar{q}N}^{inel}$. In circumstances when $\sigma_{q\bar{q}N}^{inel}$ and $\sigma_{q\bar{q}N}^{el}$ become sufficiently large, it is incorrect to ignore the contribution of $\sigma_{q\bar{q}N}^{el}$ to the total cross section. For example, $\sigma_{q\bar{q}N}^{inel}$ and $\sigma_{q\bar{q}N}^{el}$ become equal in the limit when the $q\bar{q}$ -nucleon scattering amplitude reaches its limiting value allowed by unitarity of the scattering operator.

In order to illustrate how the eikonal approximation works, we apply Eq. (2.15) in the most straightforward way by assuming it is valid at all Q^2 . Of course, as explained previously, this becomes progressively less justified as Q^2 increases because of the mixing of $|q\bar{q}\rangle$, $|q\bar{q}g\rangle$ and $|q\bar{q}gg\dots\rangle$ fluctuations of the virtual photon (in practice this restricts legitimate values of Q^2 to a few GeV^2).

As it stands, Eq. (2.15) overestimates nuclear shadowing at the higher end of the shadowing region, $0.01 \leq x \leq 0.07$. In particular, δF_2^A does not vanish at $x = 0.1$, as happens in the leading twist approximation. Thus, in order to obtain sensible results with Eq. (2.15), it is applied only for $10^{-5} \leq x \leq 0.01$. For the interval $0.01 \leq x \leq 0.1$, we assumed that δF_2^A decreases linearly and becomes zero at $x = 0.1$.

The ratio $F_2^A/(AF_2^N)$, calculated using Eq. (2.15), is presented in Fig. 12 for ^{12}C and ^{208}Pb . The Q^2 -dependence of this ratio is shown by solid ($Q = 2$ GeV), dashed ($Q = 5$ GeV) and dotted ($Q = 10$ GeV) curves. A comparison of Figs. 12 and 7 reveals the

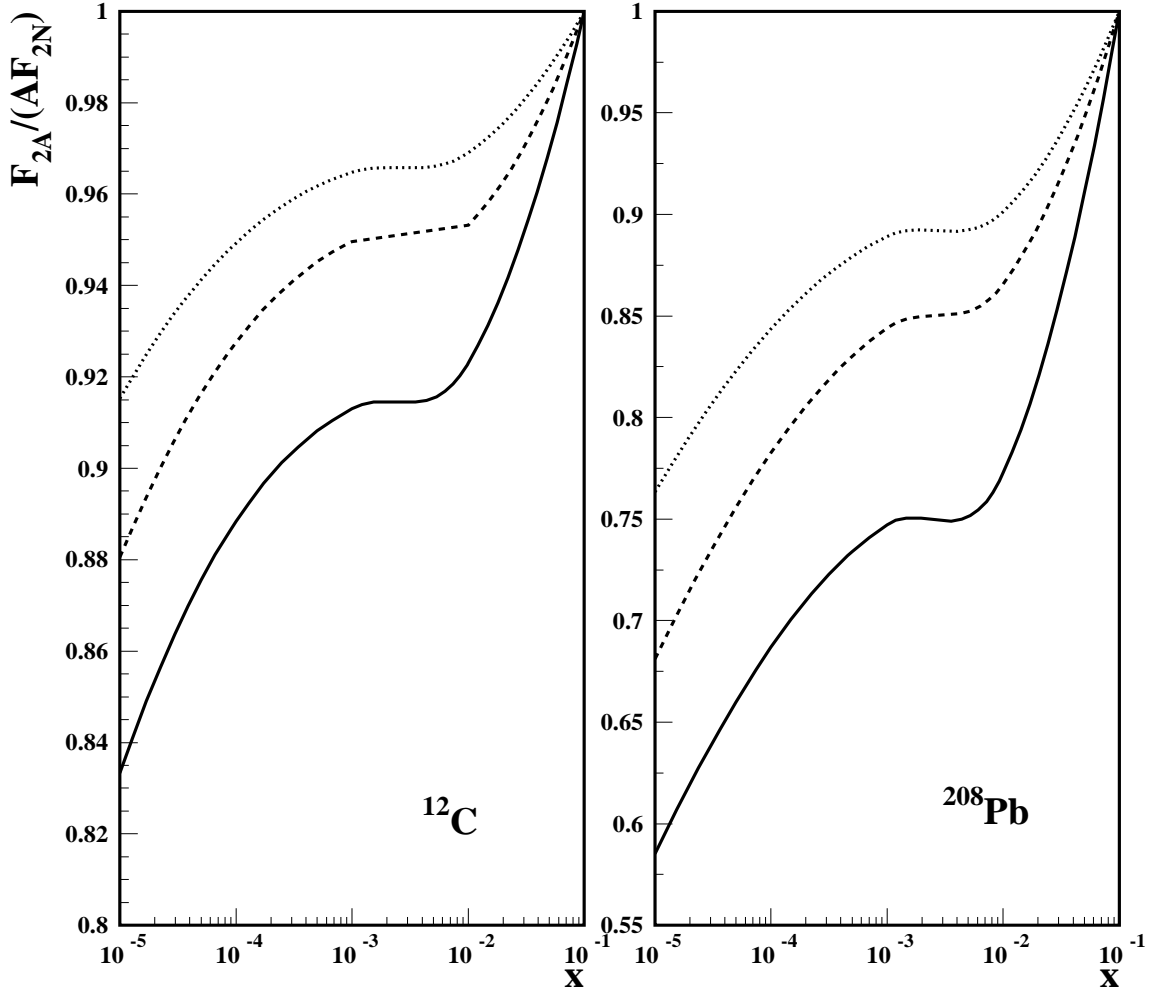


Figure 12: The ratio of nuclear to nucleon inclusive structure functions $F_2^A/(AF_2^N)$ calculated within the eikonal approximation using Eq. (2.15). The Q^2 -dependence is given by the solid ($Q = 2$ GeV), dashed ($Q = 5$ GeV) and dotted ($Q = 10$ GeV) curves.

following characteristic trends (from the considered scenarios of nuclear shadowing within the leading twist approach, we choose the one corresponding to the H1 parameterization). At $Q = 2$ GeV, and for the ^{12}C and ^{208}Pb nuclei, both leading twist and eikonal approaches give similar (within about 20%) predictions for $F_2^A/(AF_2^N)$. As Q^2 increases, for light and heavy nuclei the leading twist approximation predicts much larger shadowing than the eikonal approach. In particular, at $Q = 10$ GeV and $x = 10^{-3}$, $F_2^A/(AF_2^N)$ is shadowed more in the leading twist approach than in the eikonal approximation by 74% for ^{12}C and by 71% for ^{208}Pb . At $x = 10^{-5}$, the corresponding increase of nuclear shadowing is similar for ^{12}C and more modest for ^{208}Pb : it is 72% for ^{12}C and 49% for ^{208}Pb . The Q^2 -behaviour follows the expected pattern: while the Q^2 -behaviour of $F_2^A/(AF_2^N)$ within the leading twist approach is governed by the QCD evolution equation, and is therefore logarithmic, within the eikonal approximation it decreases with increasing Q^2 much faster and is dictated largely by the Q^2 -dependence of the virtual photon light-cone wavefunction.

2.3 Differences between the leading twist and eikonal approaches

In this subsection, we summarize what has been said so far about the differences between the leading twist and eikonal approaches to nuclear shadowing in DIS on nuclei as well as discuss problems with an unambiguous implementation of the eikonal approximation.

The two key differences, which make the approaches so distinct, are related. They are:

- a different space-time evolution of the scattering process;
- the neglect of the $|q\bar{q}g\rangle$ component (and higher Fock states) of the virtual photon in the eikonal approximation.

The eikonal approach is reliable only within the framework of non-relativistic quantum mechanics, where the number of interacting particles is conserved during collisions. In this case, the approximation that the Fock states of the incoming high-energy virtual photon can be considered frozen, is justified, and the procedure of eikonalization can be successfully carried out.

In contrast, in a quantum field theory such as QCD, the number of bare particles is not conserved. In other words, the number of effective degrees of freedom, or relevant Fock states, in the photon wavefunction depends on x and Q^2 . For example, the interacting $|q\bar{q}\rangle$ Fock state radiates gluons, thus creating and mixing with $|q\bar{q}g\rangle$, $|q\bar{q}g\dots g\rangle$ states. This mixing is properly taken into account by the QCD evolution in the leading twist approximation. Of course QED is also a quantum field theory, however, the electromagnetic coupling is much weaker than the strong coupling of QCD, and there is no self-interaction of photons, so the corrections which spoil the eikonal approximation for QCD are correspondingly much smaller in the QED case.

One immediate consequence of the contrasting space-time evolution pictures within the leading twist and eikonal approaches is the Q^2 -dependence of nuclear shadowing. As Q^2 increases, the Fock components of the virtual photon with an increasing number of gluons, $|q\bar{q}g\dots g\rangle$, become important for nuclear shadowing. This follows straightforwardly from the connection between nuclear shadowing and gluon-dominated diffraction, as found in ZEUS and H1 experiments at HERA. As a result, using the factorization theorem, the Q^2 -dependence of nuclear shadowing is governed by the DGLAP evolution equation within the leading twist approach.

In the variant of the eikonal approximation that we considered, the $|q\bar{q}g\rangle$ Fock state of the virtual photon is absent. Hence, even if one adjusts the $|q\bar{q}\rangle$ -nucleon cross section in order to reproduce correctly the nuclear structure function F_2^A at the initial scale Q_0 , the approach would necessarily underestimate nuclear shadowing at large Q^2 since the eikonal approximation is not based on QCD evolution. This was already demonstrated by comparing Figs. 12 and 7. As we will illustrate in the next section, this effect is even more dramatic for the longitudinal structure function F_L^A .

The naive formulation of the eikonal model, which only contains the $q\bar{q}$ -component of the virtual photon wavefunction, underestimates the amount of nuclear shadowing since it neglects diffractively produced inelastic states, such as $q\bar{q}g$, $q\bar{q}gg$, etc. The inclusion of a $q\bar{q}g$ component, as was done in the analysis of diffraction on the nucleon in [53], is only

a step in the right direction. In order to reproduce the correct Q^2 -behaviour of nuclear shadowing, which is governed by the DGLAP evolution equation, one should include the complete set of Fock states, i.e., an infinite series of components including infinitely many constituents.

There are several subtle points and technical problems with implementation of the eikonal approximation. Firstly, one has to be careful to use the total $q\bar{q}$ -nucleon cross section in Eq. (2.15). In the kinematics, where the elastic and inelastic $q\bar{q}$ -nucleon cross sections are compatible, the use of $\sigma_{q\bar{q}N}^{\text{inel}}$ alone would significantly underestimate nuclear shadowing.

Secondly, in order to reproduce correctly nuclear shadowing at the higher end of shadowing region, $0.01 \leq x \leq 0.07$, one needs to take into account the non-zero longitudinal momentum transfer to the nucleus through the factor $\exp(i2xm_N(z_1 - z_2))$. In order to arrive at this factor in the eikonal approximation, one needs to make a strong assumption that all essential Fock states of the virtual photon have the same invariant mass of the order of Q .

Thirdly and very importantly, there is no unambiguous way to generalize Eq. (2.15) for nuclear structure functions to something similar to Eq. (2.4) for individual nuclear parton distributions. Of course, one can attempt to replace the ratio $F_2^A/(AF_2^N)$ in Eq. (2.15) by $f_{j/A}/(Af_{j/N})$ but what can one use for cross section $\sigma_{q\bar{q}N}^{\text{tot}}$? The eikonal approximation gives no clue as to $\sigma_{q\bar{q}N}^{\text{tot}}$ for different flavors of partons. Moreover, since such a picture would not be based on the factorization theorem and QCD evolution, the scaling violations of quark and gluon nuclear distributions would not be consistent with each other and the DGLAP equations.

To conclude we would like to give a clear answer to the question as to why the eikonal approximation works so well for hadron-nucleus processes but fails for lepton-nucleus DIS processes. For high energies the hadronic projectile fluctuates into configurations which subsequently interact with the target with similar cross sections. This means that the distribution over cross section fluctuations is rather narrow. As a result, in hadron-nucleon scattering inelastic diffraction is a small correction to elastic scattering. When these ideas are applied to hadron-nucleus scattering, one sees that inelastic intermediate states (corresponding to inelastic diffraction) give a small contribution compared to elastic intermediate states (corresponding to elastic scattering). Hence, the eikonal approximation works well.

In lepton-nucleus DIS the situation is very different. Firstly, both small- and large-size fluctuations of the virtual photon contribute to DIS on the nucleon, which means that cross section fluctuations are very significant. Secondly, for small-size fluctuations, the situation for DIS off a nucleon is opposite to that assumed in the eikonal approximation: in the former the cross section for inelastic diffraction (a leading twist observable) exceeds¹⁰

¹⁰The reason for the dominance of inelastic diffraction with an increase of Q^2 at fixed small x can be traced to the definition of elastic cross section, which was introduced using t -channel factorization so that the virtual photon-target cross section has the form of the convolution of the photon ($q\bar{q}$) wavefunction with the $q\bar{q}$ -target cross section. However, as gluons are attached to the $q\bar{q}$ pair at large Q , they are predominantly emitted well before the photon wave packet has approached the target. These configurations containing gluons, which on average have a large transverse size and may be in the color octet dipole state rather than

the cross section for elastic scattering (a sub-leading twist observable). For the latter the reverse is true.

As a result, inelastic intermediate states dominate in lepton-nucleus DIS initiated by small dipoles. Of course, the presence of large-size dipoles in the virtual photon wavefunction introduces a certain degree of similarity between hadron-nucleus and lepton-nucleus scattering, but this is not sufficient to justify the application of the eikonal approximation to DIS on nuclei.

3. Nuclear shadowing of the longitudinal structure function F_L^A

As discussed above, the crucial difference between the leading twist and eikonal approaches is contrasting space-time evolution pictures of the scattering process. As a consequence, the higher Fock components of the virtual photon, containing gluons, are effectively included in the leading twist approach and are neglected in the eikonal approximation. Therefore any observable which is sensitive to the gluon distribution in the nucleus should be a good tool to distinguish between the leading twist and eikonal approximations. We have already demonstrated this using the inclusive structure function, F_2^A , at large Q^2 . An even more striking example is given by the longitudinal nuclear structure function, F_L^A , which is measured by DIS of longitudinally-polarized photons on nuclei. Other relevant processes include exclusive electroproduction of ρ (dominated by longitudinally-polarized photons) and J/ψ mesons off nuclei.

The nuclear structure function F_L^A can be obtained by a straightforward generalization of the one-loop perturbative QCD result for the nucleon [54]:

$$F_L^A(x, Q^2) = \frac{2\alpha_s(Q^2)}{\pi} \int_x^1 \frac{dy}{y} \left(\frac{x}{y}\right)^2 \left(\sum_{i=1}^{n_f} e_i^2 (1 - \frac{x}{y}) y g_A(y, Q^2) + \frac{2}{3} F_2^A(y, Q^2) \right). \quad (3.1)$$

Here n_f is the number of active quark flavors. Replacing g_A by g_N and F_2^A by F_2^N , one can present the ratio of the nuclear to nucleon longitudinal structure functions, $F_L^A/(AF_L^N)$, in the form

$$\frac{F_L^A(x, Q^2)}{AF_L^N(x, Q^2)} = \frac{\int_x^1 \frac{dy}{y} \left(\frac{x}{y}\right)^2 \left(\sum_{i=1}^{n_f} e_i^2 (1 - \frac{x}{y}) y g_A(y, Q^2) + \frac{2}{3} F_2^A(y, Q^2) \right)}{\int_x^1 \frac{dy}{y} \left(\frac{x}{y}\right)^2 \left(\sum_{i=1}^{n_f} e_i^2 (1 - \frac{x}{y}) y g_N(y, Q^2) + \frac{2}{3} F_2^N(y, Q^2) \right)}. \quad (3.2)$$

The ratio $F_L^A/(AF_L^N)$, calculated using Eq. (3.2), is presented in Fig. 13 (curves are labelled as in Fig. 5). By comparing Fig. 13 to Fig. 5 one sees that the size and Q^2 -dependence of nuclear shadowing in the ratio $F_L^A/(AF_L^N)$ are similar to those in the ratio $g_A/(Ag_N)$. Slightly smaller shadowing for $F_L^A/(AF_L^N)$ is an effect of the convolution and sea quarks present in Eq. (3.2).

in the color triplet dipole state, much more readily rescatter diffractively (i.e., with a small momentum transfer to the nucleon). As a result, the genuine total cross section of the interaction, as measured through double rescattering, turns out to be much larger at large Q^2 than the cross section defined via the elastic $q\bar{q}N$ cross section.

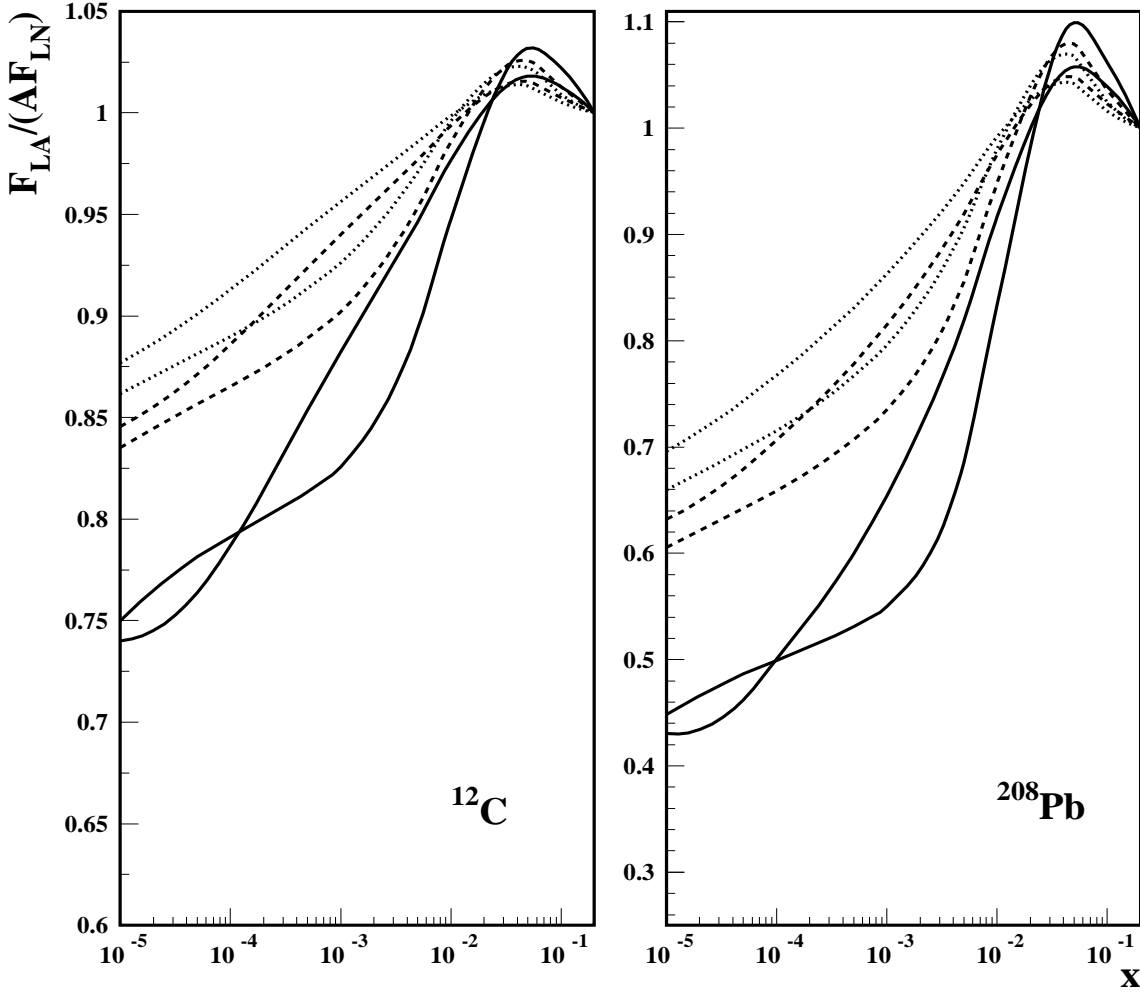


Figure 13: The ratio of nuclear to nucleon longitudinal structure functions $F_2^J/(AF_2^J)$ calculated within the leading twist approximation using Eq. (3.2). Different curves correspond to different values of Q^2 and scenarios of shadowing as in Fig. 5.

Within the eikonal approximation, one cannot use Eq. (3.2) because the eikonal approximation does not present an unambiguous scheme to evaluate g_A . Instead of Eq. (3.2), the longitudinal structure function F_L^A in the eikonal approximation can be obtained using Eq. (2.15) by replacing the helicity-averaged photon wavefunction Ψ by the longitudinally-polarized one Ψ_L :

$$|\Psi_L(\alpha, Q^2, d_t^2, m_i)|^2 = \frac{6\alpha_{em}}{\pi^2} \sum_i e_i^2 Q^2 \alpha^2 (1-\alpha)^2 K_0^2(\epsilon_i d_t) . \quad (3.3)$$

Then the ratio $F_L^A/(AF_L^N)$ can be presented in the form

$$\frac{F_L^A(x, Q^2)}{AF_L^N(x, Q^2)} = 1 - \frac{A-1}{2} \text{Re} \left[\int d\alpha d^2 d_t \sum_i |\Psi_L(\alpha, Q^2, d_t^2)|^2 \int d^2 b \int_{-\infty}^{\infty} dz_1 \int_{z_1}^{\infty} dz_2 \times \right. \\ \left. \left(\sigma_{q\bar{q}N}^{tot}(x, d_{\perp}^2, m_i) \right)^2 \rho_A(b, z_1) \rho_A(b, z_2) e^{i2xm_N(z_1-z_2)} e^{-(A/2)(1-i\eta)\sigma_{q\bar{q}N}^{tot}(x, d_{\perp}^2, m_i) \int_{z_1}^{z_2} dz \rho_A(z)} \right] /$$

$$\left(\int d\alpha d^2 d_t \sum_i |\Psi_L(\alpha, Q^2, d_t^2, m_i)|^2 \sigma_{q\bar{q}N}^{tot}(x, d_{\perp}^2, m_i) \right). \quad (3.4)$$

Results for the ratio of the longitudinal structure functions in the eikonal approximation are given in Fig. 14. As for $F_2^A/(AF_2^N)$ within the eikonal approximation, we assumed that $F_L^A/(AF_L^N)$ increases linearly for $x > 0.01$ and becomes unity at $x = 0.1$.

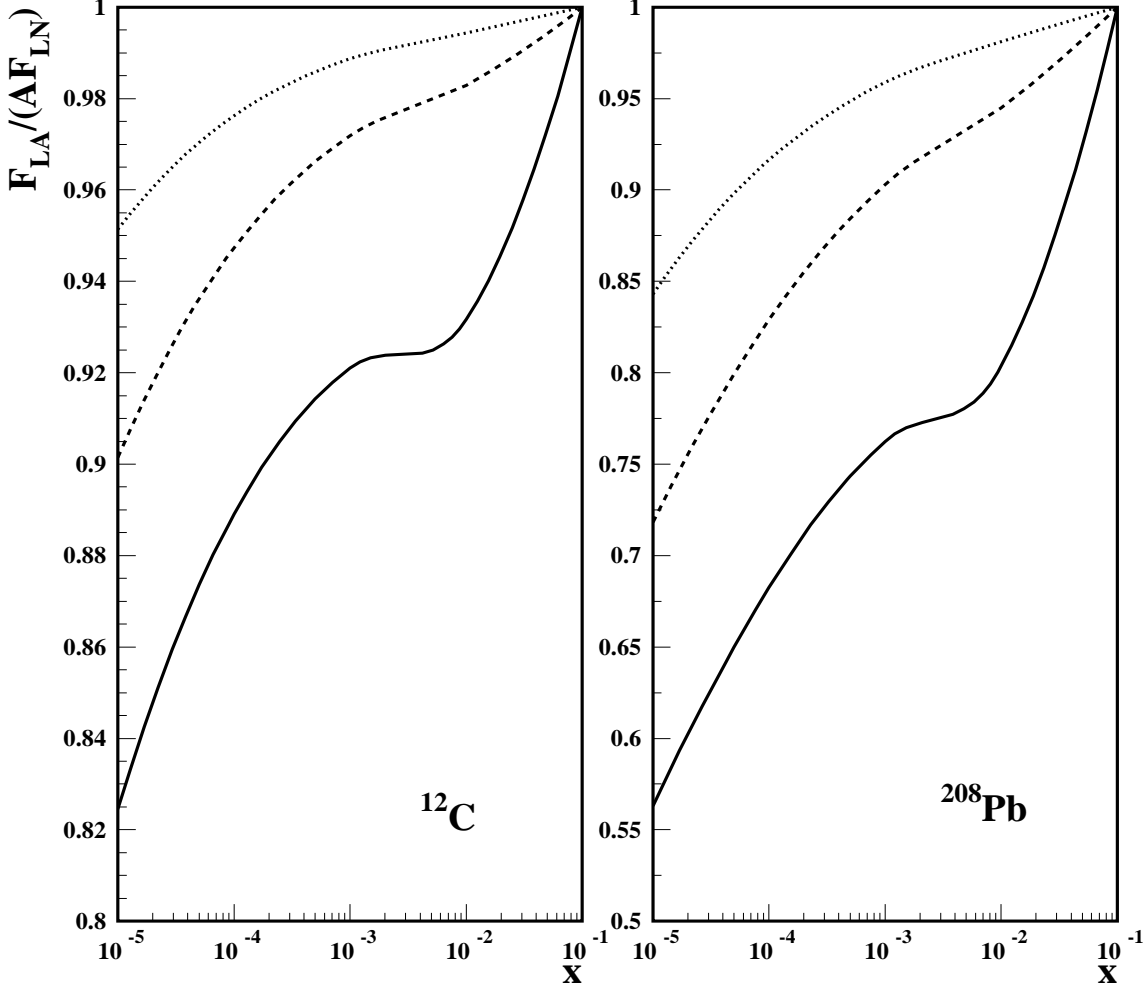


Figure 14: The ratio of nuclear to nucleon longitudinal structure functions $F_2^L/(AF_2^L)$ calculated within the eikonal approximation using Eq. (3.4). The Q^2 -dependence is shown by the solid ($Q=2$ GeV), dashed ($Q=5$ GeV) and dotted ($Q=10$ GeV) curves.

The comparison of Figs. 13 and 14 clearly reveals dramatic differences between the leading twist and eikonal approach predictions. Firstly, the leading twist approach already predicts much larger shadowing at the initial scale $Q_0 = 2$ GeV. Secondly, nuclear shadowing dies out with increasing Q^2 much faster within the eikonal approximation. In order to quantify this discussion, our results for the nuclear shadowing correction to the longitudinal structure function, $1 - F_L^A/(AF_L^N)$, of ^{12}C and ^{208}Pb are presented in Table 1 at $x = 10^{-3}$ and $x = 10^{-5}$. For the column containing the leading twist results, first values correspond to the ACWT parameterization (and the values in parenthesis to the H1 parameterization).

| | x | Q (GeV) | $1 - F_L^A/(AF_L^N)$, leading twist | $1 - F_L^A/(AF_L^N)$, eikonal |
|-------------------|-----------|-----------|--------------------------------------|--------------------------------|
| ^{12}C | 10^{-5} | 2 | 0.25 (0.26) | 0.18 |
| | | 5 | 0.16 (0.15) | 0.10 |
| | | 10 | 0.14 (0.12) | 0.049 |
| ^{12}C | 10^{-3} | 2 | 0.17 (0.12) | 0.079 |
| | | 5 | 0.098 (0.060) | 0.028 |
| | | 10 | 0.074 (0.044) | 0.011 |
| ^{208}Pb | 10^{-5} | 2 | 0.55 (0.57) | 0.43 |
| | | 5 | 0.39 (0.37) | 0.28 |
| | | 10 | 0.34 (0.30) | 0.16 |
| ^{208}Pb | 10^{-3} | 2 | 0.45 (0.35) | 0.24 |
| | | 5 | 0.26 (0.18) | 0.097 |
| | | 10 | 0.20 (0.14) | 0.041 |

Table 1: Nuclear shadowing correction to the longitudinal structure function within the leading twist and eikonal approaches.

One can see from Table 1 that, depending on x and A , the shadowing correction to F_L^A in the leading twist approach is larger, compared to the eikonal approximation, by a factor of 1.3–2 at $Q = 2$ GeV and by a factor of two to seven at $Q = 10$ GeV. Hence, measurements of F_L^A should be an excellent means to distinguish between the leading twist and eikonal approaches to nuclear shadowing.

4. Conclusions and discussion

We compare two frequently used approaches to nuclear shadowing in DIS from nuclei: the leading twist and eikonal approaches. Our comparison is based on the observation that one of the foundation principles of the two approaches, the space-time picture of the interaction, is quite different. The leading twist approach is based on the observation that at high energies the projectile interacts simultaneously with several nucleons of the nuclear target. This leads to the reference frame independent connection between nuclear shadowing in DIS from nuclei and DIS diffraction from the nucleon. The QCD factorization theorems for inclusive and diffractive scattering enable one to express the shadowing correction to the individual parton distribution functions in nuclei in terms of the corresponding diffractive parton distribution functions of the proton. Moreover, another consequence of the factorization theorems is that the scaling violations of nuclear parton distribution functions are given by the leading twist DGLAP equation.

Unlike the leading twist approach, the eikonal approximation is a frame-dependent method, which applies in the target rest frame. In this reference frame, the incoming virtual photon first fluctuates into partonic components ($|q\bar{q}\rangle$, $|q\bar{q}g\rangle$, \dots), which then interact with the nucleus. We considered the often-used approximation in which only the $|q\bar{q}\rangle$ fluctuation is considered. In this case, the $q\bar{q}$ effective dipole interacts successively and elastically with nucleons of the target. Apart from this, an additional assumption is made that such

interactions can be presented in an exponential or eikonalized form. It is important to realise that the eikonal approximation implies that only elastic ($|q\bar{q}\rangle$) intermediate states contribute to the virtual photon-nucleus cross section. In addition, the method is not based on the QCD factorization theorem and therefore does not include the proper QCD evolution.

In this work, we performed several numerical studies.

Firstly, within the leading twist approximation, the ratio of the nuclear to nucleon gluon and sea quark distribution functions was examined as a function of Bjorken x for several values of Q and for a wide range of nuclei. By testing four distinct parameterizations of diffractive parton distributions of the proton, we extended the earlier analysis of [10] and confirmed that the gluons in nuclei are shadowed more than the sea quarks. We found that the difference between gluon and sea quark nuclear shadowing was not quite as large as that found in [10] (compare Fig. 7 to Fig. 5 of [10] which uses the ACWT fit). There are two major reasons for this. Firstly the H1-type fit corresponds to a smaller diffractive gluon density at large β than ACWT. Secondly, in the current analysis we allowed for a possible difference of the slopes for the diffractive gluon and quark distributions (see appendix A for details). In addition, we made predictions for shadowing of the gluon parton distributions at central impact parameters as well as for the charm parton distributions.

Secondly, we compared predictions for the nuclear structure functions, F_2^A , within the leading twist and eikonal approximations. One should emphasize two aspects of this comparison: the size and Q^2 -dependence of the nuclear shadowing correction. At the initial scale $Q = 2$ GeV, both leading twist and eikonal approaches give similar predictions. Nevertheless, the Q^2 -dependence of F_2^A gives good discriminating power between the leading twist and eikonal approaches which reflects their conceptual differences: a logarithmic decrease of nuclear shadowing in the leading twist approach is much slower than that predicted using the eikonal approximation. For instance, at $Q = 10$ GeV and $x = 10^{-3}$, the leading twist approach predicts 71% more shadowing for $F_2^{208\text{Pb}}$ than the eikonal approximation.

Thirdly, given the fact that the eikonal approximation omits contributions of the virtual photon fluctuations containing gluons ($|q\bar{q}g\rangle, \dots$) it must predict very small nuclear shadowing for observables sensitive to the gluon distributions of nuclei. Examples of such observables include cross sections for longitudinally polarized ρ meson electroproduction, J/ψ electroproduction, and the longitudinal structure function F_L^A . We considered the latter in detail within the leading twist and eikonal approximations. The differences between the predictions for the size and Q^2 -dependence of the shadowing correction to F_L^A are very dramatic: the eikonal approximation undershoots the leading twist prediction for nuclear shadowing by at least a factor of two for all of the nuclei and values of Q^2 which we considered. Therefore, since F_L^A can be measured at the future Electron-Ion Collider [3], this observable should be able to discriminate unambiguously between the leading twist and eikonal approaches to nuclear shadowing in DIS from nuclei.

Nuclear shadowing is closely related to another interesting small- x phenomenon namely the violation of the DGLAP approximation at sufficiently small values of x . This phenomenon is referred to by various names in the literature: parton saturation, parton taming, unitarity constraints, etc. Let us consider DIS from a heavy nucleus at very large

energies, i.e., at very small x . For almost all essential impact parameters, the nuclear structure function is predicted to increase mildly with decreasing x , $F_2^A \propto \ln(1/x)$, which is significantly slower than the behaviour predicted by the DGLAP equation (see e.g., [55]). It is now understood that parton saturation and related phenomena occur in heavy nuclei at larger x than in the proton, which justifies the use of nuclear beams in attempt to study new aspects of small- x physics. On the other hand, the leading twist nuclear shadowing significantly reduces the density of partons (especially gluons) at small x and thus competes with the all-twist phenomenon of parton saturation. As a result, sensible studies of QCD at high parton densities can be carried out only if nuclear shadowing of partons is properly taken into account.

Acknowledgments

The authors are indebted to GIF, ARC, PPARC, and DOE for support. M.S. thanks J. Collins and F. Hautmann for useful discussions.

A. Parameterizations of diffractive parton distributions and σ_{eff}

Within the leading twist approach, the nuclear shadowing correction, $\delta f_{j/A}$, to nuclear PDFs is given by Eq. (2.7). It involves the effective cross section, σ_{eff}^j , which gives the strength of the interaction with any two nucleons of the nucleus leading to nuclear shadowing of the parton of flavor j . This may be expressed through the nucleon diffractive parton distribution function (DPDF) for a parton of the same flavour as follows [10, 23]:

$$\sigma_{eff}^j(x, Q^2) = \frac{16\pi}{f_{j/N}(x, Q^2)(1 + \eta^2)} \int_x^{x_{P,0}} dx_{\mathcal{P}} f_{j/N}^{D(4)}(\beta, Q^2, x_{\mathcal{P}}, t = 0) , \quad (\text{A.1})$$

where $f_{j/N}$ is the inclusive parton distribution of the nucleon; $f_{j/N}^{D(4)}$ is the diffractive parton distribution of the nucleon (which is, strictly speaking, a proton); η is the ratio of the real to imaginary parts of the diffractive scattering amplitudes. In our analysis, $\eta = 0.22$ for the amplitude corresponding to the ACWT and model 3 parameterizations and $\eta = 0.32$ when the H1 parameterization is used.

As explained in Sect. 2, the upper limit of integration, $x_{P,0}$, is different for the gluons ($x_{P,0} = 0.03$: to allow antishadowing) and for the sea quarks ($x_{P,0} = 0.1$). However, for the sea quarks, because of the factor $\exp(ix_{\mathcal{P}}m_N(z_1 - z_2))$ in Eq. (2.7) and the absence of antishadowing, the exact value of $x_{P,0}$ is unimportant for our numerical analysis.

Ignoring the small minimum momentum transfer, t_{min} , always present in inelastic diffraction, the condition $t \approx -k_t^2 = 0$ in Eq. (A.1) means that $f_{j/N}^{D(4)}$ is to be evaluated at $t = 0$. However, all the parameterizations to the diffractive data which we used are fits to t -integrated diffractive structure function $F_2^{D(3)}$. This means that we should assume a certain t -dependence of $f_{j/N}^{D(4)}$. For practical reasons, we assumed a simple exponential dependence

$$f_{j/N}^{D(4)}(\beta, Q^2, x_{\mathcal{P}}, t) = e^{-B(x_{\mathcal{P}})|t|} f_{j/N}^{D(4)}(\beta, Q^2, x_{\mathcal{P}}, t = 0) , \quad (\text{A.2})$$

where the slope B could depend on $x_{\mathbb{P}}$ (for the sea quarks) as well as on Bjorken x (for the gluons).

Introducing the diffractive distribution function $f_{j/N}^{D(3)}$ as

$$f^{D(3)}(\beta, Q^2, x_{\mathbb{P}}) \equiv \int_{-\infty}^0 dt f_{j/N}^{D(4)}(\beta, Q^2, x_{\mathbb{P}}, t), \quad (\text{A.3})$$

one readily obtains that

$$f_{j/N}^{D(4)}(\beta, Q^2, x_{\mathbb{P}}, t=0) = B(x_{\mathbb{P}}) f_{j/N}^{D(3)}(\beta, Q^2, x_{\mathbb{P}}). \quad (\text{A.4})$$

As a next step, we use the Regge factorization hypothesis which assumes that $f_{j/N}^{D(3)}$ is a product of a Pomeron flux factor, $f_{\mathbb{P}}(x_{\mathbb{P}})$, and the parton distribution functions of the Pomeron, $f_{j/\mathbb{P}}(\beta, Q^2)$:

$$f_{j/N}^{D(3)}(\beta, Q^2, x_{\mathbb{P}}) = f_{\mathbb{P}}(x_{\mathbb{P}}) f_{j/\mathbb{P}}(\beta, Q^2). \quad (\text{A.5})$$

The comparison of Eqs. (A.4) and (A.5) gives

$$f_{j/N}^D(\beta, Q^2, x_{\mathbb{P}}, t=0) = B(x_{\mathbb{P}}) f_{\mathbb{P}}(x_{\mathbb{P}}) f_{j/\mathbb{P}}(\beta, Q^2). \quad (\text{A.6})$$

Substituting Eq. (A.6) into Eq. (A.1), we obtain our master equation for σ_{eff}^j :

$$\sigma_{eff}^j(x, Q^2) = \frac{16\pi}{f_{j/N}(x, Q^2)(1 + \eta^2)} \int_x^{x_{\mathbb{P},0}} dx_{\mathbb{P}} B(x_{\mathbb{P}}) f_{\mathbb{P}}(x_{\mathbb{P}}) f_{j/\mathbb{P}}(\beta, Q^2). \quad (\text{A.7})$$

The theoretical analysis of the HERA diffractive data, in terms of quark and gluon degrees of freedom, with the additional assumption of Regge factorization and Pomeron dominance, effectively concerns itself with the parton distributions in the Pomeron, $f_{j/\mathbb{P}}(\beta, Q^2)$. One way to study $f_{j/\mathbb{P}}$ phenomenologically is to fit the experimental data by performing QCD evolution using a reasonable trial shape for $f_{j/\mathbb{P}}$ at the initial scale Q_0 . Models 1, 2 and 4, discussed below, are examples of such a determination of $f_{j/\mathbb{P}}$. Model 3 is a theoretical prediction for $f_{j/\mathbb{P}}$, which also successfully describes certain diffractive data.

It is important to emphasize that the four considered parameterizations of the gluon distribution function in the Pomeron, $f_{g/\mathbb{P}}$, become so large at small values of Bjorken x ($x < 3 \times 10^{-4}$) that the gluon-induced diffractive DIS cross section exceeds half the gluon-induced inclusive DIS cross section. Clearly, this is prohibited by the unitarity of the S matrix (when the unitarity limit is reached, the diffractive and elastic cross sections are equal each other and are equal to half the total cross section). In terms of $f_{g/\mathbb{P}}$, the unitarity restriction can be written in the form

$$\int_x^{x_{\mathbb{P},0}} dx_{\mathbb{P}} f_{\mathbb{P}}(x_{\mathbb{P}}) f_{g/\mathbb{P}}(x/x_{\mathbb{P}}, Q^2) \leq \frac{1}{2} g(x, Q^2), \quad (\text{A.8})$$

where $g(x, Q^2)$ is the number density of gluons in the nucleon. So, whenever $f_{g/\mathbb{P}}$ becomes so large as to violate the unitarity limit of Eq. (A.8), $f_{g/\mathbb{P}}$ is replaced by its limiting value

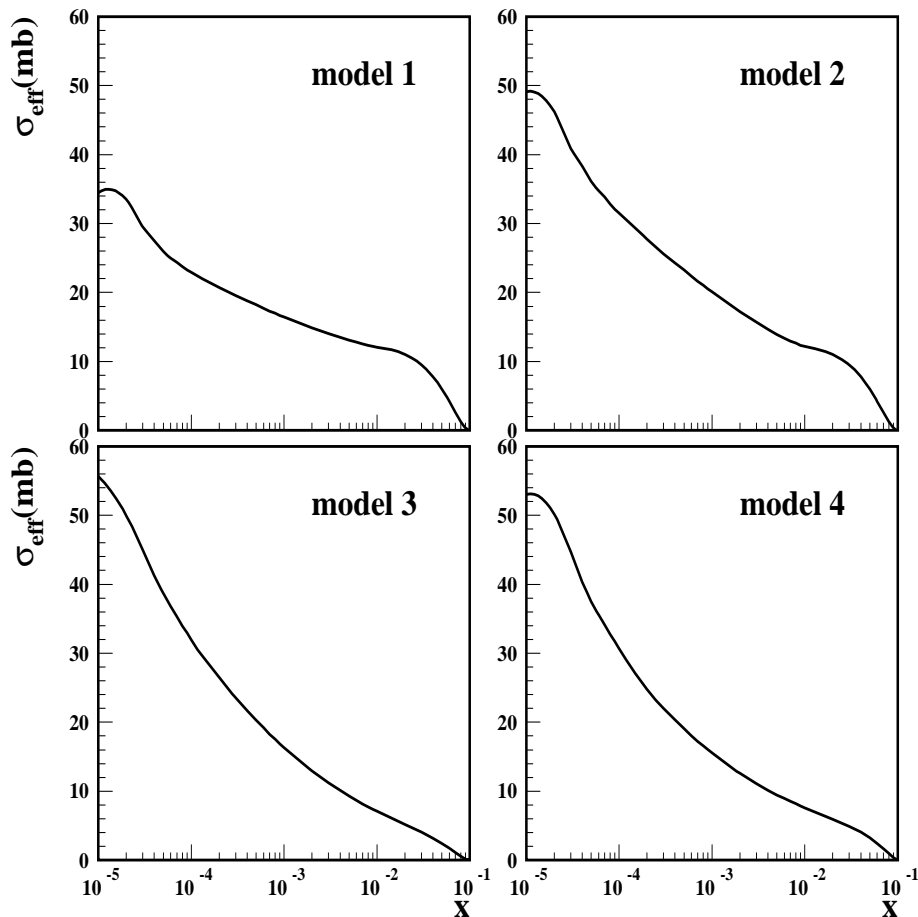


Figure 15: The effective cross section, σ_{eff}^u , for the up sea quarks obtained using Eq. (A.7) at $Q = 2$ GeV.

given by Eq. (A.7). This allows σ_{eff}^g to continue to grow as x decreases but only at a reduced rate dictated by the growth of the inclusive gluon PDF.

Predictions for σ_{eff} for the up-quark sea and gluon, obtained using Eq. (A.7) (with the unitarity restrictions on σ_{eff}^g), are presented in Figs. 15 and 16. All curves correspond to $Q = 2$ GeV. For the inclusive parton distributions, the CTEQ5M parameterization [37] was used. For the gluons, we tested two choices of the diffractive slope B_g : the solid curves correspond to B_g parametrised by Eq. (2.8), while the dotted curves are obtained with B_g of Eq. (A.12) below.

We now describe the parameterizations of DPDFs, which we used, in detail.

Model 1

Numerical predictions in [10] are based on the parameterization by Alvero, Collins, Terron and Whitmore [17]. The choice of fit D gives the best fit to the data on diffractive DIS and diffractive photoproduction of jets taken at HERA by the ZEUS and H1 collaborations. Note that this parameterization somewhat overestimates the most recent H1 data on jet production [34].

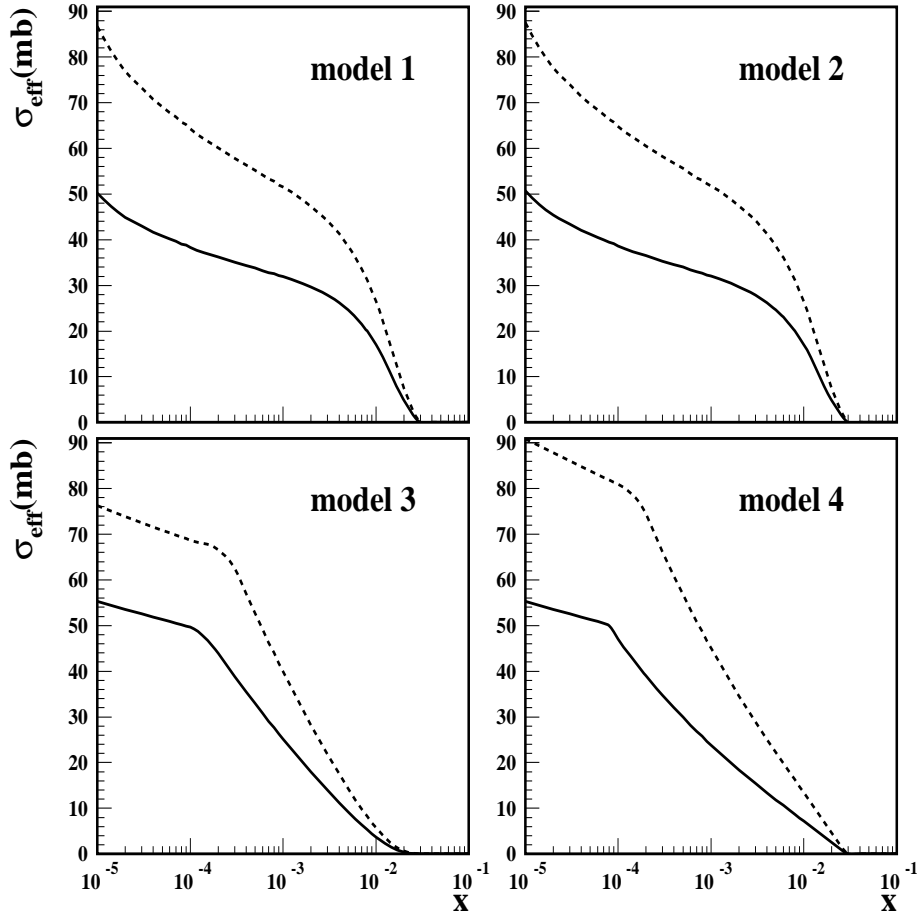


Figure 16: The effective cross section σ_{eff}^g for the gluons obtained using Eq. (A.7) (with the unitarity restriction) at $Q = 2$ GeV. The solid curves correspond to the slope B_g given by Eq. (2.8), while the dashed curves are calculated using B_g of Eq. (A.12).

The following shapes of the quark ($q = u = \bar{u} = d = \bar{d}$) and gluon parton distribution functions of the Pomeron were obtained at the initial scale $Q_0 = 2$ GeV [17]

$$\begin{aligned} \beta f_{q/\mathbb{P}}(\beta, Q_0^2) &= 0.292 \left(\beta(1 - \beta) - 0.159(1 - \beta)^2 \right) , \\ \beta f_{g/\mathbb{P}}(\beta, Q_0^2) &= 9.7\beta(1 - \beta) . \end{aligned} \tag{A.9}$$

The strange and charm quark distributions are taken to be zero at the initial scale Q_0 and are generated by QCD evolution for $Q^2 > Q_0^2$.

We would like to point out two important features of the parameterization given by Eq. (A.9). Firstly, a successful DGLAP fit to the diffractive data requires that the gluon distribution is much larger than the quark distribution, in order to reproduce the observed scaling behaviour in Q^2 . This automatically implies that σ_{eff}^g is much larger than σ_{eff}^u (e.g., compare Fig. 15 to Fig. 16 in the region around $x = 10^{-3}$). Secondly, the quark distribution is rather hard and it even becomes negative at low values of β . However, this does not lead to a paradox since the diffractive data with low β were not used in the fitting

procedure of [17]. Thus, the low- β behaviour of the parameterization (A.9) is not well constrained.

The Pomeron flux used in Eq. (A.7) was parameterized in the Donnachie-Landshoff form

$$f_{\mathcal{P}}(x_{\mathcal{P}}) = \frac{9\beta_0^2}{4\pi^2} \int_{-1}^0 dt \left[\frac{4m_p^2 - 2.8t}{4m_p^2 - t} \left(\frac{1}{1 - t/t_1} \right)^2 \right]^2 x_{\mathcal{P}}^{1-2\alpha_{\mathcal{P}}(t)} , \quad (\text{A.10})$$

where m_p is the proton mass; $\beta_0 = 1.8 \text{ GeV}^{-1}$ is the Pomeron-quark coupling; $t_1 = 0.7 \text{ GeV}^2$; $\alpha_{\mathcal{P}}(t) = \alpha_{\mathcal{P}} + \alpha' t$ is the Pomeron trajectory. The analysis of [17] showed that a successful fit the diffractive data favors $\alpha_{\mathcal{P}} = 1.14$ and $\alpha' = 0.25 \text{ GeV}^{-2}$.

The slope $B_q(x_{\mathcal{P}})$ for the quarks, which enters Eq. (A.7), was found from the t -dependence of the Pomeron flux (see Eq. (A.10))

$$B_q(x_{\mathcal{P}}) = x_{\mathcal{P}}^{1-2\alpha_{\mathcal{P}}(t=0)} / \int_{-1}^0 dt \left[\frac{4m_p^2 - 2.8t}{4m_p^2 - t} \left(\frac{1}{1 - t/t_1} \right)^2 \right]^2 x_{\mathcal{P}}^{1-2\alpha_{\mathcal{P}}(t)} , \quad (\text{A.11})$$

Thus defined $B_q(x_{\mathcal{P}})$ is a slow function of $x_{\mathcal{P}}$: B_q increases with decreasing $x_{\mathcal{P}}$. For a wide range of $x_{\mathcal{P}}$, the value of B_q is close to the slope of the diffractive structure function $F_2^{D(4)}$, $B = 7.2 \pm 1.1 \text{ GeV}^{-2}$, which was measured by the ZEUS collaboration [30].

For the gluon diffractive distribution, the slope B_g is expected to be smaller than B_q . The rationale for the use of a smaller slope for gluons in this and other models comes from two different lines of argument [56] and [57]. In [56] it was argued that $B_g \sim 5 \text{ GeV}^{-2}$ leads to effective cross sections at $Q_0 \sim 2 \text{ GeV}$ similar to that which would be obtained by rescaling the quark-antiquark dipole cross sections we found in [45] by the Casimir operator factor of $9/4$. Also we pointed out that $B_g \sim 7 \text{ GeV}^{-2}$ would lead to σ_{eff} for gluons as large as 60 mb , which would imply blackness for the interaction up to very large impact parameters. In [57], based on the calculation of the diffractive parton densities, it was argued that the size of the dipole generating the gluon diffractive parton density should be small. This would also suggest a slope closer to the case of elastic J/ψ photoproduction rather than to one expected if the soft physics dominates. Hence, in our analysis we used the x -dependent parameterization for B_g given by Eq. (2.8).

In addition, in order to access the sensitivity of our results to the uncertainty in the choice of B_g , we considered the second option, when the diffractive slopes for the gluons and quarks are the same

$$B_g = B_q , \quad (\text{A.12})$$

where B_q is given by Eq. (A.11).

Model 2

We modified the parameterizations of Eq. (A.9) by adding a low- β piece to the Pomeron parton distributions, to remove the rather unnatural feature that they go negative for small β . As a guide, we used the factorization theorem for diffractive processes. Since small values of β correspond to large diffractive masses, $M^2 \gg Q^2$, the diffractive cross section is expected to be described by formulae derived in the triple Regge limit [58] within which $W^2 \gg M^2 \gg Q^2$. One assumes in this approach that multipomeron exchanges can be

neglected. Although there are no strong theoretical reasons to support this assumption the triple Regge formulae with an effective Pomeron exchange seem to work pretty well up to rather large energies relevant for shadowing at $x \geq 10^{-4}$. In the triple Regge approximation the ratio of the diffractive cross section at $t = 0$ to total inclusive cross section in DIS should be the same as the ratio of diffractive and total cross section in real photon or hadronic diffraction. This may be expressed approximately (neglecting small corrections due to small deviations of $\alpha_{\mathcal{P}}$ from 1) as

$$\frac{d^4\sigma^{diff}/dx dQ^2 dt dM_X^2|_{t=0}}{d^2\sigma/dx dQ^2} = \frac{A}{M_X^2}, \quad (\text{A.13})$$

where the coefficient A is process-independent, with a good accuracy. Indeed, data on real photon and pion diffractive dissociation on hydrogen give $A = 0.122 \pm 0.006 \text{ GeV}^{-2}$ for the photon and $A = 0.118 \pm 0.006 \text{ GeV}^{-2}$ for the pion [59]. An earlier experiment on pion, kaon and proton diffractive dissociation on hydrogen produced similar values of A : $A = 0.102 \pm 0.013 \text{ GeV}^{-2}$ for pions at $p_{lab} = 200 \text{ GeV}/c$, $A = 0.094 \pm 0.005 \text{ GeV}^{-2}$ for protons at $p_{lab} = 200 \text{ GeV}/c$, and $A = 0.097 \pm 0.027 \text{ GeV}^{-2}$ for kaons at $p_{lab} = 100 \text{ GeV}/c$ [60]. In our analysis, we use $A = 0.12 \text{ GeV}^{-2}$.

Assuming this low- β tail appears once the quark distributions become zero, using Eq. (A.13) we arrive at the following for $\beta < \beta_0 = 0.137$:

$$\beta f_{q/\mathcal{P}}(\beta, Q_0^2) = \frac{0.02}{1-\beta} \frac{\beta_0 - \beta}{\beta_0} \quad (\text{A.14})$$

and use Eq. (A.9) for larger $\beta > \beta_0$. For the gluon channel the soft contribution is a small correction hence we ignore it and implement Eq. (A.9) for β .

Model 3

The light-cone QCD model of Hautmann, Kunszt, and Soper [35] leads to a set of the Pomeron parton densities which, upon QCD evolution in Q^2 , give a good description of the ZEUS data. The quark ($q = u = \bar{u} = d = \bar{d} = s = \bar{s}$) and gluon parton distributions in the Pomeron, at the initial scale $Q_0 = 1.5 \text{ GeV}$, read

$$\begin{aligned} \beta f_{q/\mathcal{P}}(\beta, Q_0^2) &= 0.0278\beta \left(1 + 0.824\beta - 0.286\beta^2 - 2.713\beta^3 + 1.218\beta^4 \right), \\ \beta f_{g/\mathcal{P}}(\beta, Q_0^2) &= 0.987 \left(1 + 0.821\beta - 1.495\beta^2 + 1.569\beta^3 - 0.239\beta^4 \right). \end{aligned} \quad (\text{A.15})$$

One can see from Eq. (A.15) that, in contrast to the parameterizations of Eq. (A.9), the low- β region is treated in a sensible fashion. In this model, the Pomeron flux, $f_{\mathcal{P}}$, is given by the following expression

$$f_{\mathcal{P}}(x_{\mathcal{P}}) = \frac{1}{x_{\mathcal{P}}} \left(\frac{0.0042}{x_{\mathcal{P}}} \right)^{0.253}. \quad (\text{A.16})$$

Note also that since this Pomeron flux is different from the one used in [17], a direct comparison of the overall numerical coefficients in Eq. (A.9) and Eq. (A.15) is not possible.

Model 4

The H1 collaboration performed the QCD analysis of their own data [32] and produced an independent set of $f_{j/\mathbb{P}}$. The computer code with this parameterization of $f_{j/\mathbb{P}}$ is available from [18]. One should note that this parameterization is only valid in the range $0.04 < \beta < 1$. Outside of this range, the code would give parameterizations flat in β . For illustrative and practical purposes, we fitted the quark and gluon parameterization to a simple polynomial form with a fair accuracy:

$$\begin{aligned}\beta f_{q/\mathbb{P}}(\beta, Q_0^2) &= 0.003976 - 0.02708\beta + 0.3284\beta^2 - 0.7832\beta^3 + 0.8080\beta^4 - 0.3267\beta^5, \\ \beta f_{g/\mathbb{P}}(\beta, Q_0^2) &= 0.6105 - 1.709\beta + 9.873\beta^2 - 26.49\beta^3 + 31.71\beta^4 - 13.87\beta^5.\end{aligned}\quad (\text{A.17})$$

The Pomeron flux in this model was taken in the following form

$$f_{\mathbb{P}}(x_{\mathbb{P}}) = -1.92308 \left(x_{\mathbb{P}}^{0.886} - 0.0100518 x_{\mathbb{P}}^{1.406} \right) / \left(x_{\mathbb{P}}^{2.292} (-8.84615 + \ln(x_{\mathbb{P}})) \right). \quad (\text{A.18})$$

B. Parameterization of the nuclear one-body density

| | ρ_0 (fm $^{-3}$) | c (fm) |
|-------------------|------------------------|----------|
| ^{12}C | 0.013280 | 2.2486 |
| ^{32}S | 0.0049717 | 3.3663 |
| ^{40}Ca | 0.0039769 | 3.6663 |
| ^{110}Pd | 0.0014458 | 5.308 |
| ^{197}Au | 0.0008073 | 6.5157 |
| ^{208}Pb | 0.0007720 | 6.6178 |

Table 2: The parameters entering the nuclear one-body density, $\rho_A(\vec{b}, z)$, of Eq. (B.1).

The nuclear one-body density $\rho_A(\vec{b}, z)$, which appears in Eqs. (2.2), (2.4), (2.6), (2.14)-(2.16), (3.3), (4.1) and (4.7) was parameterized in a two-parameter Fermi form

$$\rho_A(\vec{b}, z) = \frac{\rho_0}{1 + \exp[(r - c)/a]}, \quad (\text{B.1})$$

where $r = \sqrt{|\vec{b}|^2 + z^2}$ and $a = 0.545$ fm and the parameters ρ_0 and c are presented in Table 2. Also note that $\rho_A(\vec{b}, z)$ is normalized as $2\pi \int_0^\infty d|\vec{b}| \int_{-\infty}^\infty dz |\vec{b}| \rho_A(\vec{b}, z) = 1$.

References

- [1] G. Piller and W. Weise, *Phys. Rept.* **330** (2000) 1; D. F. Geesaman, K. Saito and A. W. Thomas, *Ann. Rev. Nucl. Part. Sci.* **45** (1995) 337; M. Arneodo, *Phys. Rept.* **240** (1994) 301.
- [2] D. M. Alde *et al.*, FNAL E772 Collab., *Phys. Rev. Lett.* **64** (1990) 2479; M. A. Vasilev *et al.*, FNAL E866 NuSea Collab., *Phys. Rev. Lett.* **83** (1999) 2304.
- [3] *EIC White Paper* can be found at the eRHIC home page, <http://quark.phy.bnl.gov/~raju/eRHIC.html>.
- [4] *Future physics at HERA*, Proc. of HERA workshop, Hamburg, Germany, Sept. '95-May '96, eds. G. Ingelman, A. De Roeck and R. Klanner; H. Abramowicz *et al.*, *THERA: Electron-Proton Scattering at $\sqrt{s} \sim 1$ TeV*, eds. U. Katz, M. Klein and A. Levy, in *Tesla TDR: Options*, DESY 2001-011, Vol.4, pVI-99, Hamburg 2001, ed. R. Klanner (see also <http://www.ifh.de/thera> for the THERA book).
- [5] V. N. Gribov, *Sov. Phys. JETP* **29** (1969) 483.

- [6] H. Fraas, B. Read and D. Schildknecht, *Nucl. Phys.* **B 86** (1975) 346; P. Ditsas and G. Shaw, *Nucl. Phys.* **B 113** (1976) 246; G. Shaw, *Phys. Lett.* **B 228** (1989) 125; *Phys. Rev.* **D 47** (1993) R3676.
- [7] W. Melnitchouk and A. W. Thomas, *Phys. Lett.* **B 317** (1993) 437; W. Melnitchouk and A. W. Thomas, *Phys. Rev.* **C 52** (1995) 3373; J. Kwiecinski and B. Badelek, *Phys. Lett.* **B 208** (1988) 508.
- [8] G. Piller, W. Ratzka and W. Weise, *Z. Phys. A* **352** (1995) 427.
- [9] L. Frankfurt and M. Strikman, *Phys. Rept.* **160** (1988) 235; L. L. Frankfurt and M. I. Strikman, *Nucl. Phys.* **B 316** (1989) 340.
- [10] L. Frankfurt and M. Strikman, *Eur. Phys. J. A* **5** (1999) 293.
- [11] J. Collins, *Phys. Rev.* **D 57** (1998) 3051, Erratum *Phys. Rev.* **D 61** (2000) 019902.
- [12] L. McLerran, *The Color Glass Condensate and Small x Physics: 4 Lectures*, hep-ph/0104285; R. Venugopalan, *Acta Phys. Polon.* **B30** (1999) 3731.
- [13] V. Franco and R. J. Glauber, *Phys. Rev. Lett.* **22** (1969) 370.
- [14] V. A. Abramovsky, V. N. Gribov and O. V. Kancheli, *Sov. J. Nucl. Phys.* **18** (1974) 308.
- [15] T. H. Bauer, R. D. Spital and D. R. Yennie, *Rev. Mod. Phys.* **50** (1978) 261; *ibid.* **51** (1979) 407.
- [16] V. N. Gribov and A. A. Migdal, *Sov. J. Nucl. Phys.* **8** (1969) 583.
- [17] L. Alvero *et al.*, *Phys. Rev.* **D 59** (1999) 074022.
- [18] The table of the H1 results [32] is available from <http://www-h1.desy.de/h1/www/h1work/dif/h11994.html>
- [19] J. Collins, D. Soper and G. Sterman, *Nucl. Phys.* **B 308** (1988) 833.
- [20] M. L. Good and W. D. Walker, *Phys. Rev.* **120** (1960) 1857.
- [21] L. Frankfurt, G. A. Miller and M. Strikman, *Phys. Rev. Lett.* **71** (1993) 2859.
- [22] D. R. Harrington, *Phys. Rev.* **C 52** (1995) 926.
- [23] L. Alvero, L. Frankfurt and M. Strikman, *Eur. Phys. J. A* **5** (1999) 97.
- [24] L. Frankfurt and M. Strikman, *Phys. Rept.* **160** (1988) 235.
- [25] L. L. Frankfurt, M. I. Strikman and S. Liuti, *Phys. Rev. Lett.* **65** (1990) 1725.
- [26] T. Gousset and H. J. Pirner, *Phys. Lett.* **B 375** (1996) 349.
- [27] M. Arneodo *et al.*, NMC Collab., *Nucl. Phys.* **B 481** (1996) 23.
- [28] K. J. Eskola, V. J. Kolhinen and P. V. Ruuskanen, *Nucl. Phys.* **B 535** (1998) 351.
- [29] M. Derrick *et al.*, ZEUS Collab., *Z. Physik* **C 68** (1995) 569; *Z. Physik* **C 70** (1996) 391.
- [30] J. Breitweg *et al.*, ZEUS Collab., *Eur. Phys. J. C* **1** (1998) 81.
- [31] J. Breitweg *et al.*, ZEUS Collab., *Eur. Phys. J. C* **6** (1999) 43.
- [32] C. Adloff *et al.*, H1 Collab., *Z. Physik* **C 76** (1997) 613.
- [33] C. Adloff *et al.*, H1 Collab., *Measurement of the Diffractive Structure Function $F_2^{D(3)}(\beta, Q^2, x_{\mathbb{P}})$ at HERA.*, abstract 808, parallel session 2, EPS2001, Budapest (July 2001).

- [34] C. Adloff *et al.*, H1 Collab., *Eur. Phys. J. C* **20** (2001) 29; *Z. Physik C* **74** (1997) 221.
- [35] F. Hautmann, Z. Kunszt and D. Soper, *Nucl. Phys. B* **563** (1999) 153.
- [36] C. Adloff *et al.*, H1 Collab., *Phys. Lett. B* **483** (2000) 23.
- [37] H. L. Lai *et al.*, CTEQ Collab., *Eur. Phys. J. C* **12** (2000) 375.
- [38] W. Furmanski and R. Petronzio, *Z. Physik C* **11** (1982) 293.
- [39] R. S. Thorne, Proc. 3rd UK Durham Phenomenology Workshop on HERA Physics (Durham, Sept. 1998), *J. Phys. G* **25** (1999) 1307.
- [40] M. Strikman, M. G. Tverskoi and M. B. Zhalov, *Phys. Lett. B* **459** (1999) 37.
- [41] H. Cheng and T. T. Wu, *Phys. Rev.* **186** (1969) 1611.
- [42] T. T. Chou and C. N. Yang, *Phys. Rev.* **175** (1968) 1832.
- [43] R. J. Glauber, *Phys. Rev.* **100** (1956) 242.
- [44] V. N. Gribov, *Sov. J. Nucl. Phys.* **9** (1969) 369.
- [45] M. F. McDermott *et al.*, *Eur. Phys. J. C* **16** (2000) 641.
- [46] M. F. McDermott, *The dipole picture of small x physics: a summary of the Amirim meeting*, DESY 00-126, [hep-ph/008260](#).
- [47] L. Frankfurt, W. Koepf and M. Strikman, *Phys. Rev. D* **54** (1996) 3194.
- [48] N. N. Nikolaev and B. G. Zakharov, *Phys. Lett. B* **260** (1991) 414.
- [49] B. Kopeliovich and B. Povh, *Phys. Lett. B* **367** (1996) 329.
- [50] B. Kopeliovich, J. Raufeisen and A. Tarasov, *Phys. Rev. C* **62** (2000) 035204.
- [51] E. Gotsman *et al.*, *Phys. Lett. B* **492** (2000) 47.
- [52] E. Gotsman *et al.*, *Nucl. Phys. A* **683** (2001) 383.
- [53] K. Golec-Biernat and M. Wüsthoff, *Phys. Rev. D* **60** (1999) 114023.
- [54] See for example, G. Sterman *et al.*, *The Handbook of Perturbative QCD*, *Rev. Mod. Phys.* **67** (1995) 157.
- [55] L. Frankfurt *et al.*, *Phys. Rev. Lett.* **87** (2001) 192301; L. Frankfurt *et al.*, *Electron-Nucleus Collisions at THERA*, contribution to the THERA book, eds. U. Katz, M. Klein and A. Levy, DESY-LC-REV-2001-062, [hep-ph/0104252](#).
- [56] L. Frankfurt, M. McDermott and M. Strikman, *JHEP* **103** (2001) 45.
- [57] F. Hautmann and D. E. Soper, *Phys. Rev. D* **63** (2000) 011501.
- [58] A. H. Mueller, *Phys. Rev. D* **2** (1970) 2963.
- [59] T. J. Chapin *et al.*, *Phys. Rev. D* **31** (1985) 17.
- [60] R. L. Cool *et al.*, *Phys. Rev. Lett.* **47** (1981) 701.